DOI:10.1130/B35659.1

†wqiang@gig.ac.cn.
GSA Bulletin; Month/Month 2020; v. 132; no. X/X; p. 000–000;
https://doi.org/10.1130/B35659.1; 11 figures; 1 supplemental file.
[1]Supplemental Material. **[[please provide a brief description.]]**. Please visit
https://doi.org/10.1130/GSAB.S.XXXX to access the supplemental material, and contact
editing@geosociety.org with any questions.
SCIENCE EDITOR: WENJIAO XIAO
ASSOCIATE EDITOR: YIN CHANGQING
MANUSCRIPT RECEIVED 9 FEBRUARY 2020
REVISED MANUSCRIPT RECEIVED 26 AUGUST 2020
MANUSCRIPT ACCEPTED ___ MONTH 2020
Printed in the USA

Post-collisional crustal thickening and plateau uplift of southern Tibet: Insights from Cenozoic magmatism in the Wuyu area of the eastern Lhasa block

Lu-Lu Hao[1,2], Qiang Wang[1,3,4,†], Andrew C. Kerr[5], Jin-Hui Yang[6], Lin Ma[1], Yue Qi[1], Jun Wang[1], and Quan Ou[1]

[1] State Key Laboratory of Isotope Geochemistry, Guangzhou Institute of Geochemistry, Chinese Academy of Sciences, Guangzhou 510640, China
[2] Chinese Academy of Sciences Key Laboratory of Crust-Mantle Materials and Environments, School of Earth and Space Sciences, University of Science and Technology of China, Hefei 230026, China
[3] Chinese Academy of Sciences Center for Excellence in Tibetan Plateau Earth Sciences, Beijing 100101, China
[4] College of Earth and Planetary Sciences, University of Chinese Academy of Sciences, Beijing 10049, China
[5] School of Earth and Ocean Sciences, Cardiff University, Cardiff, CF10 3YE, UK
[6] Institute of Geology and Geophysics, Chinese Academy of Science, Beijing 100029, China

ABSTRACT

The nature and timing of post-collisional crustal thickening and its link to surface uplift in the eastern Lhasa block of the southern Tibetan plateau remain controversial. Here we report on Cenozoic magmatism in the Wuyu area of the eastern Lhasa block. The Eocene (ca. 46 Ma) trachyandesites and trachydacites show slight fractionation of rare earth elements (REE), slightly negative Eu and Sr anomalies, and relatively homogeneous Sr-Nd and zircon Hf isotopes ($^{87}Sr/^{86}Sr(i)$ = 0.7050–0.7063, εNd(t) = –0.92 to –0.03, εHf(t) = +2.6 to +4.8). Previous studies have suggested Neo-Tethys oceanic slab break-off at 50–45 Ma; thus, the Wuyu Eocene magmatism could represent a magmatic response to this slab break-off and originate from relatively juvenile Lhasa crust. The Miocene (ca. 15–12 Ma) dacites and rhyolites have adakitic affinities, e.g., high Sr (average 588 ppm), Sr/Y (29–136), and La/Yb (30–76) values, low Y (4–12 ppm) and Yb (0.4–0.9 ppm) contents, and variable Sr-Nd and zircon Hf isotopes ($^{87}Sr/^{86}Sr(i)$ = 0.7064–0.7142, εNd(t) = –11.7 to –3.7, εHf(t) = –3.2 to +4.5). Their more enriched Sr-Nd-Hf isotopes relative to the Eocene lavas indicate that they should be derived from mixed Lhasa lower crust comprising juvenile crust, ultrapotassic rocks, and probably Indian lower crust-

derived rocks. This study has also revealed the transformation from Eocene juvenile and thin crust with a thickness of < 40 km to Miocene mixed and thickened crust with a thickness of > 50 km. Combined with published tectonic data, we suggest that both lithospheric shortening and magma underplating contributed to eastern Lhasa block post-collisional crustal thickening. Given the spatial-temporal distribution of eastern Lhasa block magmatism and regional geology, we invoke a post-collisional tectonic model of steep subduction of the Indian plate and subsequent westward-propagating plate break-off beneath the eastern Lhasa block, which caused the surface uplift.

INTRODUCTION

Surface uplift of a mountain belt or plateau is commonly thought to be controlled primarily by crustal thickening (e.g., Dewey and Bird, 1970; Molnar, 1988; Bird, 1991; DeCelles et al., 2002; Chen et al., 2018) or deep dynamic processes (e.g., lithospheric mantle thinning, subduction dynamics) (e.g., England and Houseman, 1988; Molnar et al., 1993; Turner et al., 1993; Chung et al., 1998; Currie et al., 2005; Husson et al., 2014). The Tibetan plateau is one of the largest and highest plateaus on Earth and is therefore ideal for studying the progress of, and the mechanism(s) responsible for, surface uplift. Nevertheless, the mechanism(s) of post-collisional uplift of the southern Tibetan plateau remain(s) unclear (e.g., Turner et al., 1993; Williams et al., 2001; DeCelles et al., 2002; Chung et al., 1998, 2005; Husson et al., 2014; Webb et al., 2017). For example, post-collisional (< 40 Ma) surface uplift of the eastern Lhasa block east of 87°E in southern Tibet is generally ascribed to crustal thickening (e.g., Chung et al., 2009; Zhu et al., 2017) based on the abundance of post-collisional adakitic intrusions and porphyries (e.g., Chung et al., 2003; Hou et al., 2004).

However, three key points need clarification to help verify this crustal thickening model. Firstly, an assumption of this model is that the post-collisional adakitic rocks were derived from thickened Lhasa lower crust. However, various genetic models have been proposed for these rocks, including (1) partial melting of the Neo-Tethys oceanic slab (Qu et al., 2004) or thickened Lhasa lower crust (Chung et al., 2003; Hou et al., 2004; Guo et al., 2007) or subducted Indian lower crust (Xu et al., 2010; Zheng et al., 2012); (2) crustal assimilation with fractional crystallization (AFC) of basaltic magmas (Gao et al., 2007); and (3) mixing of ultrapotassic and juvenile crust-derived magmas (Zhang et al., 2014). Secondly, the process and mechanism of crustal thickening remains unclear. For example, Chung et al. (2009) emphasized the collision between the Indian plate and the Lhasa block, which induced significant contraction and thickening of the Lhasa block. However, Mo et al. (2007) and Zhu et al. (2017) suggested that the early Cenozoic (60–45 Ma) crustal thickening of the Lhasa block was mainly caused by basaltic magma underplating as a result of Neo-Tethys oceanic slab break-off, while post-collisional (< 40 Ma) crustal thickening was largely a consequence of tectonic thickening due to intra-continent thrusting and subducted Indian plate underplating. The question of whether magma underplating contributed to post-collisional crustal thickening remains unresolved (Ji et al., 2012; DePaolo et al., 2019). Thirdly, the relationship between crustal thickening and plateau uplift remains unclear. Crustal thickening has been associated with plateau elevation based on the principle of isostasy (Watts, 2001). However, this simple link has recently been challenged by several studies (e.g., Leary et al., 2017; Deng and Jia, 2018). For example, Leary et al. (2017) proposed that wet and well-vegetated conditions with relatively low elevations existed in the India-Asia suture zone at ca. 40 Ma **[[Should this instead be ~40 m.y.?]]** after the start of collision and at least ca. 25 Ma **[[Should this instead be ~25 m.y.?]]** after major crustal

shortening in the region. Collectively, the nature and mechanism of post-collisional crustal thickening in the eastern Lhasa block and its link to surface uplift remain uncertain.

In this study we have reassessed the Cenozoic (Eocene and Miocene) volcanic rocks in the Wuyu area along the southern margin of the eastern Lhasa block (Fig. 1). Our work shows that both Eocene lavas and Miocene adakitic rocks were generated by partial melting of Lhasa lower crust and so can be used to track post-collisional crustal thickening. On the basis of our new data and published results, we propose a geodynamic model for generating post-collisional magmatism in the Lhasa block. This model can explain the link between geodynamics, post-collisional crustal thickening, and surface uplift of southern Tibet.

GEOLOGICAL SETTING AND SAMPLES

From south to north the Himalayan-Tibetan orogen consists of the Himalaya, Lhasa, Qiangtang, and Songpan-Ganze blocks, and these are separated from each other by the Indus-YarlungZangbu, Bangong-Nujiang, and Jinsha sutures, respectively (Fig. 1). The Lhasa block in southern Tibet was the last terrane to be accreted onto Eurasia in the late Mesozoic before its collision with the northward-drifting Indian plate during the early Cenozoic (e.g., Yin and Harrison, 2000; Zhu et al., 2013).

The prolonged northward subduction of the Indus-YarlungZangbu (Neo-Tethys) Ocean resulted in significant intrusive and extrusive magmatism in the Lhasa block during the Triassic to Late Cretaceous. Initial collision between India and Eurasia (India-Lhasa) was proposed to have occurred in the early Cenozoic (65–55 Ma) (e.g., Yin and Harrison, 2000; DeCelles et al., 2011). The Indian continental plate was dragged downward by the subducting oceanic slab during the subsequent ongoing collision (e.g., Zhu et al., 2015). The buoyancy of the Indian plate would counteract the effects of the oceanic slab pull, eventually resulting in the separation of the oceanic and continental lithosphere (i.e., oceanic slab break-off) at ca. 50–45 Ma (e.g., Chemenda et al., 2000; Kohn and Parkinson, 2002; Mahéo et al., 2002, 2009).

During the period from initial collision to oceanic slab break-off, the syn-collisional Linzizong volcanic succession and coeval granitoids were formed (Mo et al., 2007) on the central and southern Lhasa sub-blocks (Fig. 1). The Linzizong volcanic succession extends for > 1200 km along the Lhasa block and is divided into the lower Dianzhong, middle Nianbo, and upper Pana Formations with ages of ca. 69–60 Ma, 56–54 Ma, and 52–43 Ma, respectively (Lee et al., 2012). After oceanic slab break-off, the collision zone evolved to a post-collisional intra-continental setting with Indian plate subduction beneath the Lhasa block (Mo et al., 2007). Numerous studies (e.g., Chung et al., 2005) have identified a ca. 40–26 Ma magmatic gap in the western Lhasa block (west of 87°E). In contrast, minor magmatic rocks have been reported in the eastern Lhasa block during this period (Harrison et al., 2000; Zheng et al., 2012; Guan et al., 2012; Jiang et al., 2014; Ma et al., 2017), e.g., ca. 38 Ma Wolong granites, ca. 35 Ma Quguosha gabbros, and ca. 30–26 Ma Zedang granitoids, which are proposed to represent prolonged magmatism as a result of oceanic slab break-off (Hou et al., 2012).

Following this period, magmatism in the Lhasa block became much more prevalent and is characterized by the 25–8 Ma potassic-ultrapotassic and 30–10 Ma adakitic rocks (Fig. 1). The potassic lavas are distributed sporadically in the Xungba, Konglong, and Yangying areas (e.g., Miller et al., 1999). The ultrapotassic lavas were previously only found in the western Lhasa block (e.g., Coulon et al., 1986; Turner et al., 1996; Williams et al., 2001, 2004; Zhao et al., 2009; Guo et al., 2015), but recent studies have identified further occurrences in the eastern Lhasa block, e.g., in the Bairong (90°E) and Zhunuo areas (87°30′E) (e.g., Xu et al., 2017; Sun et al., 2018). The adakitic rocks commonly occur as intrusions and porphyries and are commonly

found along the southern margin of the eastern Lhasa block (Fig. 1B), and minor lava outcrops (e.g., at Yare and Dajiaco) have been reported in the western Lhasa block (e.g., Williams et al., 2001).

The present study focuses on the eastern Lhasa block's Wuyu Basin, ~200 km west of Lhasa City, where the Wuyu Group crops out at the basin margins and is distributed in an elliptical area extending NE–SW (Fig. 1C). The Wuyu Group contains the Miocene Gazhacun Formation in the lower part and the Pliocene Zongdangcun Formation in the upper part. The Gazhacun Formation mainly consists of the felsic volcanic rocks and minor sandstones while the Zongdangcun Formation primarily consists of the sandstones and conglomerates. The Gazhacun Formation rests on the Linzizong volcanic succession across an angular unconformity and conformably underlies the Zongdangcun Formation. Zhou et al. (2010) reported a K-feldspar Ar-Ar age (42.9 ± 2.5 Ma) for the Linzizong volcanic succession. Ar-Ar dating of biotite and plagioclase indicates that the lavas in the Gazhacun Formation were erupted at 15–12 Ma (Spicer et al., 2003; Zhou et al., 2010). To date, no zircon ages have been reported for Wuyu Cenozoic magmatism.

We collected the Wuyu lava samples from a transect that crosses the Eocene Linzizong volcanic succession and Miocene Gazhacun Formation (Fig. 1C). The Eocene lavas are trachyandesites and trachydacites, whereas the Miocene lavas are mainly dacites and rhyolites. All samples are porphyritic and contain phenocrysts of biotite, plagioclase, and quartz in variable proportions and groundmass of plagioclase, quartz, and glass (Fig. 2). We focused on the petrogenesis and geochemical variations of Wuyu Cenozoic lavas in order to assess the mechanism of eastern Lhasa block post-collisional crustal thickening and its link to plateau uplift.

METHODS AND RESULTS

Whole-rock major- and trace-element and Sr-Nd isotope analyses and laser ablation-multicollector-inductively coupled plasma-mass spectrometry (LA-MC-ICP-MS) zircon Hf isotope analyses were carried out at the State Key Laboratory of Isotope Geochemistry, Guangzhou Institute of Geochemistry, Chinese Academy of Sciences (CAS), Guangzhou, China. LA-ICP-MS zircon U-Pb dating was conducted at the Institute of Geology and Geophysics, Chinese Academy of Sciences, Beijing, China. A more detailed discussion of the methodology and the analytical results is presented in the Appendix.

LA-ICP-MS Zircon U-Pb Ages

One Linzizong volcanic succession trachydacite sample (NML01-1) and two Gazhacun Formation dacite samples (NML04-1 and NML05-2) were chosen for zircon U-Pb dating (Figs. 3A–3C). Zircons from these samples are euhedral and long-to-short prismatic with average lengths of ~250 μm and length-to-width ratios of 3:1. Most of the zircons are transparent and colorless and show clear oscillatory zoning, which indicates a magmatic origin.

Twenty-two analyses of zircons from NML01-1 are concordant, yielding a weighted mean $^{206}Pb/^{238}U$ age of 45.6 ± 0.7 Ma (mean square of weighted deviates [MSWD] = 0.72), which is broadly consistent with the K-feldspar Ar-Ar age (ca. 42.9 ± 2.5 Ma) (Zhou et al., 2010). According to Lee et al. (2012), the Wuyu Linzizong volcanic succession lavas are ca. 46 Ma and belong to the Pana Formation.

Zircons from samples NML04-1 and NML05-2 yield weighted mean $^{206}Pb/^{238}U$ ages of 12.3 ± 0.3 Ma and 11.7 ± 0.3 Ma, respectively. These ages, combined with the Ar-Ar dating of biotite and plagioclase (15–12 Ma) (Spicer et al., 2003; Zhou et al., 2010), confirm that the Wuyu Gazhacun Formation lavas are mid-Miocene in age.

DOI:10.1130/B35659.1

Whole-Rock Major and Trace Elements

The Wuyu Eocene lavas have SiO_2 contents of 58.8–69.1 wt.% and high (K_2O + Na_2O) contents of 7.9–9.2 wt.%; therefore, they classify as trachyandesite and trachydacite on the total alkali-silica (TAS) diagram (Fig. 4A). They have high K_2O contents of 3.9–5.0 wt.% and belong to the high-K calc-alkaline series (Fig. 4B). These rocks have low MgO (< 1.6 wt.%) and form clearly continuous major element variation arrays with the Pana Formation calc-alkaline rock suite (Lee et al., 2012) (Fig. 5). The Wuyu Eocene lavas show slight enrichment in light rare earth elements (LREE) on chondrite-normalized rare earth element (REE) plots (Fig. 6A) with $(La/Yb)_N$ = 10.8–13.6, where N indicates chondrite-normalized (Sun and McDonough, 1989). They also have flat, heavy REE (HREE) patterns with $(Gd/Lu)_N$ = 1.5–1.8 and slightly negative Eu anomalies (Eu/Eu* = 0.65–0.89). Their primitive mantle-normalized (Sun and McDonough, 1989) trace-element patterns (Fig. 6B) are characterized by enrichment in large ion lithophile elements (LILEs) (e.g., Rb, Th, and Ba) and depletion in high field strength elements (HFSEs) (e.g., Nb and Ta) and Sr. The Wuyu Eocene lavas and Pana Formation calc-alkaline rock suite have similar REE and trace element distribution patterns (Figs. 6A–6B).

The Wuyu Miocene dacites and rhyolites have high SiO_2, Na_2O, and K_2O contents and belong mainly to the high-K calc-alkaline series (Fig. 4). They have relatively low MgO, TiO_2, Fe_2O_3, Cr, and Ni contents (Appendix). Their chondrite-normalized REE patterns (Fig. 6A) show significant fractionation of REEs with $(La/Yb)_N$ = 21.2–54.3 and slightly to negligibly negative Eu anomalies (Eu/Eu* = 0.62–0.92). Primitive mantle-normalized trace element patterns (Fig. 6B) for these rocks are characterized by enrichment in the LILEs and depletion in the HFSEs with slightly negative to positive Sr anomalies. The Wuyu Miocene lavas have similar REE and trace-element patterns as post-collisional adakitic rocks in the Lhasa block (Figs. 6A–6B). Major- and trace-element features (e.g., Fig. 6) of the Wuyu Miocene lavas indicate their adakitic affinities (Castillo, 2012), e.g., high SiO_2 (58.1–75.9 wt.%), Al_2O_3 (13.3–17.3 wt.%), and Sr (139–1014 ppm with an average of 588 ppm, mostly > 400 ppm) contents, low Y (4–12 ppm) and Yb (0.4–0.9 ppm) contents, and high Sr/Y (29–136) and $(La/Yb)_N$ (21–54) ratios.

Whole-Rock Sr-Nd Isotopes

The Wuyu Eocene lavas have relatively homogeneous Sr-Nd isotopic compositions with $^{87}Sr/^{86}Sr(i)$ = 0.7050–0.7063 and εNd(46 Ma) = –0.92 to –0.03 and have similar compositions to the calc-alkaline suite of the Pana Formation (Lee et al., 2012) (Fig. 7). In contrast, the Miocene Wuyu adakitic rocks have variable and more enriched Sr-Nd isotopic signatures with $^{87}Sr/^{86}Sr(i)$ = 0.7064–0.7142 and εNd(12 Ma) = –11.7 to –3.7, similar to post-collisional adakitic rocks elsewhere in the Lhasa block (Fig. 7).

Zircon Hf Isotopes

Hf isotopes were analyzed on zircon grains in the same domains in which U-Pb ages were measured. Twenty analyses of zircons from the Wuyu Eocene lava NML01-1 show relatively homogeneous $^{176}Hf/^{177}Hf$ ratios of 0.282816–0.282880, which correspond to εHf(t) values of +2.6 to +4.8 (Fig. 3D). These are the first reported zircon Hf isotopes of the Pana Formation in the southern Lhasa sub-block, and the values are similar to those of the Dianzhong and Nianbo Formations of the Linzizong volcanic succession (Lee et al., 2007) (Fig. 3D). Analyses of zircons from the Wuyu Miocene adakitic rocks, NML04-1 and NML05-2, show $^{176}Hf/^{177}Hf$ ratios of 0.282675–0.282874 and 0.282743–0.282893, which correspond to εHf(t) values of –3.2 to +3.9 and –0.8 to +4.5, respectively (Fig. 3D). The zircon Hf isotopes of the Wuyu Miocene adakitic rocks are similar to those of the post-collisional adakitic rocks elsewhere in the Lhasa block (Fig. 3D).

DISCUSSION

Petrogenesis of Wuyu Magmatism

Wuyu Eocene Lavas

An important observation is that the major element variations, trace element patterns, and Sr-Nd isotopic compositions of the Wuyu Eocene lavas imply a close genetic link to the Pana Formation calc-alkaline basaltic-intermediate-acidic rock suite (Lee et al., 2012) (Figs. 4–7). Therefore, the Wuyu lavas and the Pana calc-alkaline suite can be considered together in terms of their petrogenesis. Thus, it is feasible to suggest that the Wuyu Eocene felsic lavas could be derived from the Pana Formation basaltic rocks by various processes such as magma mixing, AFC, or re-melting of underplated basaltic rocks.

The Wuyu Eocene lavas have the highest silica contents among the Pana Formation calc-alkaline suite, and this would seem to preclude a petrogenetic origin by magma mixing. They have broadly same Sr-Nd isotopes as the Pana Formation calc-alkaline basic rocks, which indicates negligible crustal assimilation during their generation. Significant mineral fractionation (e.g., plagioclase) can also be ruled out given that it would yield increasingly negative Eu anomalies with increasing SiO_2, which is not observed in the Wuyu Eocene lavas (Fig. 8A). The greater volume of felsic rocks in the Pana Formation calc-alkaline suite also argues against their generation via fractional crystallization (FC) process, which commonly produces smaller amounts of the evolved silicic magmas (Mo et al., 2008). Furthermore, on a plot of La versus La/Yb (Fig. 8B), the compositions of these rocks plot along the path of partial melting rather than FC. Thus, we prefer to suggest melting of underplated basaltic rocks (i.e., intrusive equivalents of Pana Formation basalts) as an explanation for the generation of the Wuyu Eocene lavas. This is consistent with their zircon Hf isotopes of +2.6 to +4.8, which suggests juvenile components in their sources.

Significantly, zircon Hf isotope mapping (Hou et al., 2015) has identified the juvenile crustal block that was formed by Neo-Tethys oceanic subduction, particularly in the southern margin of the eastern Lhasa block. However, the Wuyu Eocene lavas and Pana Formation calc-alkaline suite have slightly more enriched Sr-Nd isotopes than do arc rocks (Fig. 7D). This enrichment thus suggests that Indian crust may have released fluids into the mantle wedge during the syn-collisional stage (Mahéo et al., 2009). This indicates that the Wuyu Eocene lavas were generated by partial melting of relatively juvenile Lhasa crust. The relatively juvenile Lhasa crust was formed during a protracted Neo-Tethys oceanic subduction and was slightly modified by a shorter Indian continental subduction during the syn-collisional stage. As reviewed above, continuing collision following the initial impact of Lhasa and India in the early Cenozoic eventually induced Neo-Tethys oceanic slab break-off at ca. 50–45 Ma (e.g., Zhu et al., 2015; Ji et al., 2016). Accordingly, the Wuyu Eocene (ca. 46 Ma) lavas may represent a magmatic response to this oceanic slab break-off.

Wuyu Miocene Adakitic Rocks

Several models have been proposed for generating adakitic rocks, including AFC of mantle-derived magmas (Castillo et al., 1999; Macpherson et al., 2006), magma mixing (Streck et al., 2007), and partial melting of either oceanic crust (e.g., Defant and Drummond, 1990; Gutscher et al., 2000), subducted continental crust (e.g., Wang et al., 2008), or thickened lower continental crust (Atherton and Petford, 1993; Mahéo et al., 2009; Pang et al., 2016).

The ultrapotassic rocks, as the only post-collisional mantle-derived magmas in the Lhasa block (e.g., Zhao et al., 2009; Chung et al., 2005), have much more enriched Sr-Nd isotopes than post-collisional adakitic rocks (Figs. 7D). Thus, assimilation of, or mixing with, juvenile crust by

basic magmas may represent a possible model for the formation of adakitic rocks. However, this model is not supported by the variation of SiO_2 with Nd and Sr isotopes for the Wuyu adakitic rocks (Figs. 7A–7B). Furthermore, a positive correlation between K_2O/Na_2O and SiO_2 (Fig. 4C) argues against their generation by mixing between ultrapotassic and crust-derived magmas, given that ultrapotassic melts have clearly lower SiO_2 and higher K_2O/Na_2O than crust-derived melts. In addition, their Dy/Yb ratios decrease with increasing SiO_2 (Fig. 8C), which argues against high-pressure garnet fractionation from basic magmas (Macpherson et al., 2006).

The post-collisional adakitic rocks in the Lhasa block have variable and high-K contents and enriched Sr-Nd isotopes. These signatures are inconsistent with an oceanic slab origin, which generally yields adakites with low K_2O contents and mid-oceanic-ridge, basalt-like depleted Sr-Nd isotopes (e.g., Defant and Drummond, 1990; Castillo, 2012). In addition to this, numerous studies have argued that, following the India-Lhasa collision, the Neo-Tethys oceanic slab detached from the Indian continental slab at ca. 45 Ma and sunk into the deep mantle during the Eocene (DeCelles et al., 2002; Mahéo et al., 2009). This being the case, the oceanic slab may not be a feasible candidate for the source of Lhasa Oligocene-Miocene adakitic rocks.

The post-collisional adakitic rocks in the Lhasa block have clearly distinct Sr-Nd isotopes in comparison to the Himalayan late Oligocene-Miocene leucogranites ($^{87}Sr/^{86}Sr(i) > 0.730$ and $\varepsilon Nd(t) < -10$). These leucogranites were generated by re-melting of Himalayan upper crustal schists and gneisses (e.g., King et al., 2007**[[King et al., 2007, is not in the reference list.]]**) (Fig. 7C). Furthermore, the post-collisional adakitic rocks have high K_2O/Na_2O (up to 7) and different Sr-Nd isotopes compared to those of the Himalayan Eocene adakites ($K_2O/Na_2O \leq 1$) (Figs. 4 and 7D), which were generated by partial melting of the Indian lower crust and mid-crustal amphibolites (Zeng et al., 2011; Hou et al., 2012). Thus, the post-collisional adakitic rocks in the Lhasa block were unlikely to have been generated by partial melting of subducted Indian continental crust. Furthermore, Lhasa adakitic rocks have relatively low MgO (< 3 wt.%) (Fig. 8D), Cr (< 70 ppm), and Ni (< 50 ppm) contents. These compositions are inconsistent with adakitic rocks with high Cr, Ni, and MgO that are derived from melts of subducted continental crust that have interacted with overlying mantle (Wang et al., 2006).

As discussed above, the zircon Hf isotope mapping has revealed the juvenile crustal block, especially along the southern margin of the eastern Lhasa block (e.g., Hou et al., 2015; Zhu et al., 2015) (Fig. 7), formed by the protracted Neo-Tethys oceanic subduction. For example, pre-collisional (ca. 80 Ma) lower crust-derived adakitic rocks in the eastern Lhasa block (Wen et al., 2008) have depleted Sr-Nd isotopes. The Linzizong volcanic succession rocks and coeval granitoids could represent juvenile crust formed during the syn-collisional stage, and the majority of them have $\varepsilon Nd(t) > 0$ (Mo et al., 2007). Some of the Linzizong volcanic succession rocks (e.g., the Pana Formation lavas), as discussed above, have slightly more enriched Sr-Nd isotopes than oceanic subduction-related juvenile crust, suggesting minor contributions of Indian crust-released fluids into the mantle wedge during the syn-collisional stage (Mahéo et al., 2009). However, the Lhasa post-collisional adakitic rocks have much more enriched Sr-Nd isotopes than the juvenile crust (including the Pana Formation). On an initial $^{87}Sr/^{86}Sr$ vs $\varepsilon Nd(t)$ diagram (Fig. 7D), the Lhasa post-collisional adakitic rocks plot on a mixing trend between an end-member isotopically similar to the juvenile crust and an end-member similar to Lhasa post-collisional ultrapotassic rocks or Indian Eocene adakites and their lower-middle crust sources (Zeng et al., 2011; Hou et al., 2012). The high K_2O and K_2O/Na_2O values of the post-collisional adakitic rocks (Fig. 4) may indicate significant contributions of ultrapotassic rocks in their sources, though Indian lower crust-derived magma contributions cannot be ruled out.

The Lhasa post-collisional adakitic rocks yielded some negative zircon εHf(t) values, which are consistent with the more negative εHf(t) values of the ultrapotassic lavas (Fig. 3D). Significantly, it has been shown repeatedly that underplating of post-collisional ultrapotassic magmas beneath the eastern Lhasa block has played a key role in crustal reworking, porphyry Cu ore formations, and crust-mantle magma mixing (e.g., Yang et al., 2014**[[Yang et al., 2014, is not in the reference list. 2015 here?]]**; Hou et al., 2015; Sun et al., 2018; Wang et al., 2018; Hao et al., 2019a). Thus, we propose that the Lhasa post-collisional adakitic rocks were most likely generated by partial melting of mixed and thickened Lhasa lower crust, which was composed of relatively juvenile crust, ultrapotassic rocks, and probably Indian lower crust-derived magmas.

Post-Collisional Geodynamics of Southern Tibet

As noted above, after Neo-Tethys oceanic slab break-off at ca. 45 Ma, the Himalaya-Tibet collision zone became a post-collisional intra-continental setting (e.g., Chung et al., 2005). Three main geodynamic processes have been considered to play key roles in generating post-collisional magmatism in south Tibet: (1) thinning of the lithospheric mantle beneath the Tibetan plateau (Houseman et al., 1981; Turner et al., 1993; Williams et al., 2001; Chung et al., 2005); (2) Indian continental subduction (Ding et al., 2003; Zhao et al., 2009); and (3) break-off of subducted Indian continental lithospheric slab (Chemenda et al., 2000; Mahéo et al., 2002, 2009; Williams et al., 2004).

Models that invoke lithospheric mantle thinning propose that the Indian continental slab was unable to move further downward after oceanic slab break-off due to both the more buoyant nature of the Indian continental slab relative to the Asian lithosphere and a lack of slab pull. Accordingly, the continuous northward impingement of India resulted in significant contraction of the Lhasa lithospheric mantle that may have been thermally weakened and softened by previous arc and syn-collisional magmatism (Chung et al., 2005; Chen et al., 2017). The gravitational instability produced in response to lithospheric thickening would have resulted in lithospheric mantle thinning (wholesale mantle delamination or convective removal of the lithosphere basal layer) (Houseman et al., 1981; Houseman and Molnar, 1997; Conrad and Molnar, 1999).

During lithospheric mantle thinning, the sinking lithosphere would have been replaced by hot, rising asthenospheric mantle. The juxtaposition of hot mantle against either the remaining lithospheric mantle and/or lower crust would trigger melting in these overlying domains (Turner et al., 1992). In the case of southern Tibet, convective removal of only a part of Asian lithospheric mantle has been invoked due to the occurrence of enriched, mantle-derived ultrapotassic magmas (e.g., Chung et al., 2005). However, an important limitation of the convective thinning model is related to the size and distribution of magmatic activity. Igneous rocks related to lithospheric convective thinning are usually spread over regional and broad domains (see Mahéo et al., 2009, for review). This contrasts with the localized linear belt distribution of post-collisional magmatism in southern Tibet and its western prolongation, the south Karokorum (150 km wide and more than 2000 km long) (Mahéo et al., 2002, 2009). Furthermore, we recently identified the first post-collisional A-type magmatism of the Himalayan-Tibetan orogen in the Lhasa block (Hao et al., 2019b), which strongly indicates a direct link between north-south extensional tectonics (e.g., the Main Central thrust and South Tibetan detachment system and the Kailas Basin) and the deep mantle process generating the post-collisional magmatism. These geological events straddled the Himalaya and Lhasa blocks and can be easily reconciled with break-off of subducted Indian continental slab (DeCelles et al.,

2011; Leary et al., 2016; Hao et al., 2019b) (as discussed below) rather than lithospheric mantle thinning. Thus, our preferred model is that Indian continental slab continued to subduct northward beneath the Lhasa block after the Neo-Tethys oceanic slab break-off.

The continental subduction model has the advantage of accounting for the extent of magmatism along a narrow zone parallel to the Indus–Yarlung Zangbo suture zones (IYSZ) (e.g., Ding et al., 2003; Mahéo et al., 2009). As discussed above, continental subduction was already active at 60–45 Ma (e.g., Chung et al., 2005), resulting in the more enriched Sr-Nd isotopes of the Pana Formation relative to oceanic subduction arc rocks (Fig. 7D). Therefore, the change in isotopic compositions between the southern Tibetan ultrapotassic rocks and the Pana Formation could reflect a greater contribution from Indian continent-released fluids and melts in post-collisional mantle sources (Mahéo et al., 2009). However, this continuous continental subduction cannot easily account for the limited or absent magmatism during 40–30 Ma. Furthermore, continental subduction always proceeds at low thermal gradients and thus represents cold subduction (e.g., Zheng, 2019), resulting in cooling of the base of the wedge due to thermal conduction from the cold slab. Thus, continental subduction generally requires additional geodynamic processes to produce post-collisional magmas, e.g., roll-back or break-off. Geophysical data reveal two shallower anomalies beneath the India-Asia convergence zone (Van derVoo et al., 1999), which have been attributed to detachment of northward-subducted Neo-Tethys oceanic lithosphere and Indian continental lithosphere (DeCelles et al., 2002; Replumaz et al., 2010). This may indicate Indian continental slab break-off.

In the model of Indian continental slab break-off (e.g., DeCelles et al., 2011; Leary et al., 2016; Hao et al., 2019b) (Fig. 9), part of the subducted Indian lithosphere becomes detached, thereby creating a gap into which asthenospheric mantle can rise and trigger partial melting of Indian continental slab and Asian mantle wedge metasomatized by subducted Indian crust-released melts and fluids. The intrusion of mantle melts into the crust-induced partial melting of thickened and mixed Lhasa lower crust (juvenile crust, ultrapotassic rocks, and probably Indian lower crust-derived magmas) to generate the post-collisional adakitic rocks.

Such a tectonic model of Indian continental slab break-off would have developed along orogen-perpendicular cross sections and thus cannot explain the along-strike variations of post-collisional magmatism along the length of southern Tibet (e.g., Webb et al., 2017). For example, eastern Lhasa block post-collisional magmatism was restricted to the eastern Lhasa block southern margin while western Lhasa block post-collisional magmatism covers a relatively broad distribution that includes the Lhasa sub-block (Fig. 1B). In addition to this, at ca. 40–26 Ma magmatism and magmatic gap occurred in the eastern Lhasa block and western Lhasa block, respectively. Therefore, several studies (Leary et al., 2016; Webb et al., 2017) have highlighted a need for a three-dimensional evolutionary model for the India-Asia orogen. In Figure 10 we have adapted the 3D model for Indian continental subduction to illustrate the tectonic setting of post-collisional magmatism in the Lhasa block. The different spatial distributions of post-collisional magmatism (Fig. 1B) may reflect low-angle subduction of the Indian plate beneath the western Lhasa block that reaches far beneath the central Lhasa sub-block (e.g., DeCelles et al., 2011; Leary et al., 2016; Webb et al., 2017; Wang et al., 2018; Hao et al., 2018, 2019b) and relatively steep subduction for a short distance beneath the eastern Lhasa block (Hou et al., 2012) (Fig. 10A). Similar scenarios of subduction segmentation were suggested to have occurred in the Peru area of the Andes (e.g., Gutscher et al., 1999).

The tectonic model of Indian plate flat subduction and subsequent foundering beneath the western Lhasa block has been recently demonstrated in detail for the post-collisional evolution of

the western Lhasa block-Himalaya orogen (Hao et al., 2019b). In the western Lhasa block case, Indian plate low-angle/flat subduction is compatible with the 40–25 Ma **[[OK?]]** magmatic gap because it would have prevented asthenosphere-derived heating and led to cooling of western Lhasa block mantle and crust (Chung et al., 2005). Subsequent ca. 25 Ma (ultra)potassic magmatism and coeval north-south extensional tectonics could be ascribed to foundering and break-off of the Indian continental slab (e.g., DeCelles et al., 2011; Hao et al., 2019b).

Steep subduction of the Indian continental slab beneath the eastern Lhasa block is consistent with not only the restricted distribution along the IYSZ for post-collisional adakitic magmatism, but also the ca. 40–26 Ma magmatism along the Lhunze-Yalaxiangbo-Zedong traverse, which becomes younger to the north and ceases at ca. 30–26 Ma (Hou et al., 2012). Asthenospheric upwelling after oceanic slab break-off would melt the front edge of the subducted Indian continental plate (Hou et al., 2012; Zhang et al., 2014). Magmatism along with steep subduction (i.e., persistent plunging of Indian slab into the mantle beneath the eastern Lhasa block) would show a northward younging trend and eventually cease when the Indian slab subducted into the deep mantle and obstructed asthenospheric upwelling (Hou et al., 2012). Subsequent east-west 30–10 Ma magmatism in the eastern Lhasa block could have been caused by break-off of this steep Indian continental slab. During Indian continental slab break-off (Fig. 9), the asthenospheric mantle can rise and trigger partial melting of the Indian continent and Asian mantle wedge metasomatized by subducted Indian crust-released melts and fluids. Magma underplating and tectonic shortening contributed to crustal thickening. The intrusion of mantle melts into the crust induced partial melting of mixed and thickened Lhasa lower crust (juvenile crust, ultrapotassic rocks, and probably Indian lower crust-derived magmas) to generate the adakitic rocks. This magmatism initiated at 30–26 Ma near the eastern Himalayan syntaxis (Linzhi area) (Chung et al., 2003; Pan et al., 2012; Zhang et al., 2014) and systematically decreases in age to the west to ca. 10 Ma near the Xigaze area (Webb et al., 2017). This east-to-west younging trend could likely reflect westward-propagating break-off of subducted Indian continental slab beneath the eastern Lhasa block (Pan et al., 2012; Zhang et al., 2014; Leary et al., 2016; Webb et al., 2017) (Fig. 10B).

Post-Collisional Crustal Thickening of Southern Tibet

As discussed above, both the Eocene lavas and Miocene adakitic rocks in the Wuyu area were generated by partial melting of the Lhasa lower crust. Their geochemical characteristics can therefore be used to constrain the mineral assemblages of the crustal source rocks. Given that plagioclase is strongly enriched in Sr and Eu, and garnet is strongly depleted in LREEs and enriched in HREEs and Y (Rapp et al., 2003**[[Rapp et al., 2003, is not in the reference list.]]**; Wang et al., 2016), low Sr/Y and La/Yb ratios (Fig. 11) and slightly negative Eu and Sr anomalies of the Wuyu Eocene rocks could reflect a plagioclase-rich source with little or no garnet. In contrast, high Sr/Y and La/Yb ratios (Fig. 11), slightly negative to negligible Eu anomalies, and slightly negative to positive Sr anomalies of the Wuyu Miocene rocks could reflect a garnet-rich source containing little or no plagioclase. Increases in Sr/Y and La/Yb ratios of the Wuyu rocks from Eocene to Miocene, and temporal variations in mineral assemblages of the crustal source rocks, suggest post-collisional crustal thickening in the Wuyu area between the Eocene and Miocene. Several geochemical indicators (e.g., Sr/Y, La/Yb) in magmatic rocks have been used as proxies for crustal thickness (e.g., Chung et al., 2009; Chaharlang et al., 2020). Notably, the La/Yb ratio is less sensitive to differences in crustal thickness of 25–45 km, yet it can clearly show when crustal thickness exceeds ~50 km (DePaolo et al., 2019). In the Wuyu case, the crustal thickness in the Eocene can be estimated to be < 40 km based on their low

La/Yb ratios (< 20). The elevated La/Yb ratios in the Miocene adakitic rocks indicate that the crustal thickness is > 50 km. This is consistent with experimental petrology data (e.g., Xiong, 2006) indicating that adakitic rocks could be produced by partial melting of garnet-bearing mafic rocks at depths of > 50 km in the lower crust.

Furthermore, numerous studies have demonstrated the crustal thickening of the Lhasa block in the period ca. 50–40 Ma and ca. 30–25 Ma, i.e., the period between the late stage of the Linzizong volcanic succession volcanism and the beginning of the adakitic magma emplacement (Mo et al., 2007; Chung et al., 2009; Zhu et al., 2017; DePaolo et al., 2019). Additionally, on the basis of the Nd isotopes and La/Yb ratios of Gangdese granitoids, DePaolo et al. (2019) concluded that the southern margin of the eastern Lhasa block (south of 29.8°N latitude) was relatively thin, ~25–35 km thick until 45 Ma, but was thickened substantially to at least 55–60 km (based on Nd isotopes) and possibly as much as 70–75 km (based on La/Yb) by 30 Ma. Our results, indicating that the crustal thickness of the Wuyu area (~29.7°N, Appendix) was < 40 km and > 50 km in the Eocene and Miocene, respectively, are strongly consistent with the conclusions of DePaolo et al. (2019). Moreover, our rock samples are from just one transect, which clearly demonstrates this post-collisional crustal thickening. Notably, this post-collisional crustal thickening is mainly restricted to the relatively narrow region between the present IYZS suture and ~30°N in the eastern Lhasa block , which was considered to be ascribed to the steep subduction of Indian continental slab beneath the eastern Lhasa block. In addition, as noted above, the Indian continental slab continued to subduct beneath the Lhasa block after oceanic slab break-off, and Lhasa lithospheric delamination (wholesale lithospheric mantle and a part of crust) would be unlikely to occur (Mahéo et al., 2009). Thus, the southern eastern Lhasa block most probably experienced a single stage of crustal thickening from Eocene to Miocene.

Various mechanisms have been proposed to explain eastern Lhasa block post-collisional crustal thickening. For instance, Chung et al. (2005, 2009) suggested that the stage of post-collisional crustal thickening corresponded to the apparent magmatic gap and emphasized that the intensity of the collision between the Indian plate and the Lhasa block induced significant contraction and thickening of the latter. In addition to this, Zhu et al. (2017) suggested that eastern Lhasa block post-collisional (< 40 Ma) crustal thickening was largely a consequence of tectonic thickening due to intra-continent thrusting and subducted Indian plate underplating. Here, we also propose that tectonic shortening contributed to crustal thickening as indicated by tectonic data. For example, significant thrust belts began to be widely emplaced in the IYSZ and southern Lhasa block during the post-collisional stage, e.g., ca. 30–23 Ma Gangdese Thrust (GT) (Yin et al., 1994, 1999), ca. 25–10 Ma Great Counter Thrust (GCT) (Harrison et al., 2000). This is a strong indication of crustal shortening and thickening at that time. Indeed, van Hinsbergen et al. (2011) have constrained ~40 km of N-S shortening of the Lhasa block to the 50–20 Ma period.

This study has revealed that Lhasa post-collisional adakitic rocks have not only higher Sr/Y and La/Yb but also more evolved Sr-Nd-Hf isotopes than the Eocene rocks. This could reflect the transformation from Eocene relatively thin and juvenile crust with thickness < 40 km to late Oligocene-Miocene thickened and mixed crust (juvenile crust, ultrapotassic rocks, and probably Indian lower crust-derived magmas) with thickness > 50 km. Thus, in addition to tectonic shortening, magma underplating beneath the eastern Lhasa block could also play a key role in eastern Lhasa block post-collisional crustal thickening.

Post-Collisional Surface Uplift of Southern Tibet

Stable isotope-based and paleobotanical paleoaltimeters have been used to quantitatively study surface uplift of the Tibetan plateau after India-Asia collision (e.g., Spicer et al., 2003; Currie et al., 2005; DeCelles et al., 2007; Ding et al., 2014, 2017; Deng and Ding, 2015; Su et al., 2019). Two high mountains of Qiangtang and Gangdese (> 4500 m) that sandwiched a low elevation Lunpola-Nima Basin should occur in Tibet in the early Cenozoic (e.g., Ding et al., 2014; Su et al., 2019). Moreover, the Himalayas also have low elevations of ~1 km in the late Paleocene (e.g., Ding et al., 2017). Thus, it has been widely proposed that the wholesale "Roof of the World" Tibetan plateau has only been developing from the late Oligocene–early Miocene (Deng and Ding, 2015; Liu et al., 2016; Su et al., 2019). However, the mechanism of this post-collisional uplift remains unclear.

The contribution of post-collisional crustal thickening to eastern Lhasa block uplift has been widely proposed (e.g., DeCelles et al., 2002; Zhu et al., 2017). However, this study has demonstrated eastern Lhasa block significant post-collisional crustal thickening since the early Eocene. This may not explain why the plateau uplift took place in late Oligocene–early Miocene. Furthermore, modeling of Husson et al. (2014) indicates that the northward subduction of the Indian plate beneath the Asian plate would result in tectonic shortening but no significant surface uplift due to subduction traction of the Indian slab. Conversely, Indian slab break-off beneath the eastern Lhasa block could remove downward pull to switch the compressional stress in a collision zone to tensional stress (Lim and Kidd, 2007; Husson et al., 2014). With this release of slab dynamic traction and the relative southward translation of the slab weight, the range uplifted toward isostatic equilibrium and topography across the orogen increased (Webb et al., 2017). Thus, we propose that eastern Lhasa block post-collisional uplift could be most likely caused by the propagating slab break-off of Indian slab beneath the eastern Lhasa block since 30 Ma. Similar scenarios have been proposed in several orogens, e.g., the Romagnan Apennines and New York-Vermont-Quebec Taconic orogens (van der Meulen et al., 1999; Lim and Kidd, 2007).

CONCLUSIONS

(1) Both Eocene lavas and Miocene adakitic rocks in the Wuyu area of the eastern Lhasa block (eastern Lhasa block) were generated by partial melting of Lhasa lower crust.

(2) Comparisons of trace-elemental and Sr-Nd-Hf isotopic characteristics between Eocene and Miocene rocks indicate the transformation from Eocene thin and juvenile crust with thickness < 40 km to Miocene thickened and mixed crust (juvenile crust, ultrapotassic rocks, and probably Indian lower crust-derived magmas) with thickness > 50 km.

(3) Both tectonic shortening and magma underplating contributed to eastern Lhasa block post-collisional (< 40 Ma) crustal thickening.

(4) Eastern Lhasa block post-collisional magmatism can be ascribed to Indian plate steep subduction and subsequent westward-propagating break-off beneath the eastern Lhasa block, which could cause the surface uplift for the thick eastern Lhasa block of the southern Tibetan plateau.

ACKNOWLEDGMENTS

We thank Science Editor Wenjiao Xiao, Associate Editor Yin Changqing, and three anonymous reviewers for their thoughtful reviews and constructive comments that greatly improved the manuscript. Financial support for this research was provided by the Second Tibetan Plateau Scientific Expedition and Research (STEP) (2019QZKK0702), the National Natural Science Foundation of China (No. 41630208, 41802048, and 91855215), the Strategic Priority Research Program (A) of the Chinese Academy of Sciences (grant no. XDA2007030402), the

Key Program of the Chinese Academy of Sciences (QYZDJ-SSW-DQC026), the National Key R and D Program of China (No. 2016YFC0600407), the Key Program of Guangzhou City (No. 201604910124), and the Guangzhou Institute of Geochemistry, Chinese Academy of Sciences (GIGCAS 135 project 135TP201601). This is contribution No. IS-~~XXXX~~ **[[Fill in number?]]** from GIGCAS.

REFERENCES CITED

Atherton, M.P., and Petford, N., 1993, Generation of sodium-rich magmas from newly underplated basaltic crust: Nature, v. 362, p. 144–146, https://doi.org/10.1038/362144a0.

Bird, P., 1991, Lateral extrusion of lower crust from under high topography in the isostatic limit: Journal of Geophysical Research: Solid Earth, v. 96, p. 10275–10286, https://doi.org/10.1029/91JB00370.

Castillo, P.R., 2012, Adakite petrogenesis: Lithos, v. 134–135, p. 304–316, https://doi.org/10.1016/j.lithos.2011.09.013.

Castillo, P.R., Janney, P.E., and Solidum, R.U., 1999, Petrology and geochemistry of Camiguin Island, southern Philippines: Insights to the source of adakites and other lavas in a complex arc setting: Contributions to Mineralogy and Petrology, v. 134, no. 1, p. 33–51, https://doi.org/10.1007/s004100050467.

Chaharlang, R., Ducea, M., and Ghalamghash, J., 2020, Geochemical evidences for quantifying crustal thickness over time in the Urumieh-Dokhtar magmatic arc (Iran): Lithos, v. 374–375, no. 105723, https://doi.org/10.1016/j.lithos.2020.105723.

Chemenda, A.I., Burg, J.P., and Mattauer, M., 2000, Evolutionary model of the Himalaya-Tibet system: Geopoem based on new modelling, geological and geophysical data: Earth and Planetary Science Letters, v. 174, p. 397–409, https://doi.org/10.1016/S0012-821X(99)00277-0.

Chen, J.L., Yin, A., Xu, J.F., Dong, Y.H., and Kang, Z.Q., 2018, Late Cenozoic magmatic inflation, crustal thickening, and >2 km of surface uplift in central Tibet: Geology, v. 46, p. 19–22, https://doi.org/10.1130/G39699.1.

Chen, M., Niu, F., Tromp, J., Lenardic, A., Lee, C.A., Cao, W., and Ribeiro, J.M., 2017, Lithospheric foundering and underthrusting imaged beneath Tibet: Nature Communications, v. 8, no. 15659, https://doi.org/10.1038/ncomms15659.

Chung, S.L., Lo, C.H., Lee, T.Y., Zhang, Y.Q., Xie, Y.W., Li, X.H., Wang, K.L., and Wang, P.L., 1998, Diachronous uplift of the Tibetan plateau starting 40 Myr ago: Nature, v. 394, p. 769–773, https://doi.org/10.1038/29511.

Chung, S.L., Liu, D.Y., Ji, J.Q., Chu, M.F., Lee, H.Y., Wen, D.J., Lo, C.H., Lee, T.Y., Qian, Q., and Zhang, Q., 2003, Adakites from continental collision zones: Melting of thickened lower crust beneath southern Tibet: Geology, v. 31, p. 1021–1024, https://doi.org/10.1130/G19796.1.

Chung, S.L., Chu, M., Zhang, Y., Xie, Y., Lo, C., Lee, T., Lan, C., Li, X., Zhang, Q., and Wang, Y., 2005, Tibetan tectonic evolution inferred from spatial and temporal variations in post-collisional magmatism: Earth-Science Reviews, v. 68, p. 173–196, https://doi.org/10.1016/j.earscirev.2004.05.001.

Chung, S.L., Chu, M.F., Ji, J.Q., O'Reilly, S.Y., Pearson, N.J., Liu, D.Y., Lee, T.Y., and Lo, C.H., 2009, The nature and timing of crustal thickening in southern Tibet: Geochemical and zircon Hf isotopic constraints from postcollisional adakites: Tectonophysics, v. 477, p. 36–48, https://doi.org/10.1016/j.tecto.2009.08.008.

595 Conrad, C.P., and Molnar, P., 1999, Convective instability of a boundary layer with temperature-
596 and strain-rate-dependent viscosity in terms of 'available buoyancy': Geophysical Journal
597 International, v. 139, p. 51–68, https://doi.org/10.1046/j.1365-246X.1999.00896.x.
598 Coulon, C., Maluski, H., Bollinger, C., and Wang, S., 1986, Mesozoic and Cenozoic volcanic
599 rocks from central and southern Tibet: ^{39}Ar-^{40}Ar dating, petrological characteristics and
600 geodynamical significance: Earth and Planetary Science Letters, v. 79, p. 281–302,
601 https://doi.org/10.1016/0012-821X(86)90186-X.
602 Currie, B., Rowley, D., and Tabor, N., 2005, Middle Miocene paleoaltimetry of southern Tibet:
603 Implications for the role of mantle thickening and delamination in the Himalayan orogen:
604 Geology, v. 33, p. 181–184, https://doi.org/10.1130/G21170.1.
605 DeCelles, P.G., Robinson, D.M., and Zandt, G., 2002, Implications of shortening in the
606 Himalayan fold-thrust belt for uplift of the Tibetan plateau: Tectonics, v. 21, no. 6, p. 12-1–
607 12-25, https://doi.org/10.1029/2001TC001322.
608 DeCelles, P.G., Quade, J., Kapp, P., Fan, M., Dettman, D.L., and Ding, L., 2007, High and dry in
609 central Tibet during the Late Oligocene: Earth and Planetary Science Letters, v. 253, p. 389–
610 401, https://doi.org/10.1016/j.epsl.2006.11.001.
611 DeCelles, P.G., Kapp, P., Quade, J., and Gehrels, G.E., 2011, Oligocene-Miocene Kailas basin,
612 southwestern Tibet: Record of postcollisional upper-plate extension in the Indus-Yarlung
613 suture zone: Geological Society of America Bulletin, v. 123, p. 1337–1362,
614 https://doi.org/10.1130/B30258.1.
615 Defant, M.J., and Drummond, M.S., 1990, Derivation of some modern arc magmas by melting of
616 young subducted lithosphere: Nature, v. 347, p. 662–665, https://doi.org/10.1038/347662a0.
617 Deng, L., and Jia, G., 2018, High-relief topography of the Nima basin in central Tibetan plateau
618 during the mid-Cenozoic time: Chemical Geology, v. 493, p. 199–209,
619 https://doi.org/10.1016/j.chemgeo.2018.05.041.
620 Deng, T., and Ding, L., 2015, Paleoaltimetry reconstructions of the Tibetan plateau: Progress and
621 contractions: National Science Review, v. 2, p. 417–437,
622 https://doi.org/10.1093/nsr/nwv062.
623 DePaolo, D.J., Harrison, T.M., Wielicki, M., Zhao, Z., Zhu, D.C., Zhang, H., and Mo, X., 2019,
624 Geochemical evidence for thin syn-collision crust and major crustal thickening between 45
625 and 32 Ma at the southern margin of Tibet: Gondwana Research, v. 73, p. 123–135,
626 https://doi.org/10.1016/j.gr.2019.03.011.
627 Dewey, J.F., and Bird, J.M., 1970, Mountain belts and the new global tectonics: Journal of
628 Geophysical Research, v. 75, p. 2625–2647, https://doi.org/10.1029/JB075i014p02625.
629 Ding, L., Kapp, P., Zhong, D., and Deng, W., 2003, Cenozoic volcanism in Tibet: Evidence for a
630 transition from oceanic to continental subduction: Journal of Petrology, v. 44, p. 1833–1865,
631 https://doi.org/10.1093/petrology/egg061.
632 Ding, L., Xu, Q., Yue, Y.H., Wang, H.Q., Cai, F.L., and Li, S., 2014, The Andean-type
633 Gangdese Mountains: Paleoelevation record from the Paleocene-Eocene Linzhou Basin:
634 Earth and Planetary Science Letters, v. 392, p. 250–264,
635 https://doi.org/10.1016/j.epsl.2014.01.045.
636 Ding, L., Spicer, R.A., Yang, J., Xu, Q., Cai, F., Li, S., Lai, Q., Wang, H., Spicer, T.E.V., Yue,
637 Y., Shukla, A., Srivastava, G., Khan, M., Bera, S., and Mehrotra, B., 2017, Quantifying the
638 rise of the Himalaya orogen and implications for the South Asian monsoon: Geology, v. 45,
639 no. 3, p. 215–218, https://doi.org/10.1130/G38583.1.

England, P., and Houseman, G., 1988, The mechanics of the Tibetan plateau: Philosophical Transactions of the Royal Society A, v. 326, p. 301–320.

Gao, Y., Hou, Z., Kamber, B.S., Wei, R., Meng, X., and Zhao, R., 2007, Adakite-like porphyries from the southern Tibetan continental collision zones: Evidence for slab melt metasomatism: Contributions to Mineralogy and Petrology, v. 153, p. 105–120, https://doi.org/10.1007/s00410-006-0137-9.

Guan, Q., Zhu, D., Zhao, Z., Dong, G., Zhang, L., Li, X., Liu, M., Mo, X., Liu, Y., and Yuan, H., 2012, Crustal thickening prior to 38 Ma in southern Tibet: Evidence from lower crust-derived adakitic magmatism in the Gangdese Batholith: Gondwana Research, v. 21, p. 88–99, https://doi.org/10.1016/j.gr.2011.07.004.

Guo, Z., Wilson, M., and Liu, J., 2007, Post-collisional adakites in south Tibet: Products of partial melting of subduction-modified lower crust: Lithos, v. 96, p. 205–224, https://doi.org/10.1016/j.lithos.2006.09.011.

Guo, Z., Wilson, M., Zhang, M., Cheng, Z., and Zhang, L., 2015, Post-collisional ultrapotassic mafic magmatism in south Tibet: Products of partial melting of pyroxenite in the mantle wedge, induced by roll-back and delamination of the subducted Indian continental lithosphere slab: Journal of Petrology, v. 56, no. 7, p. 1365–1406, https://doi.org/10.1093/petrology/egv040.

Gutscher, M., Olivet, J., Aslanian, D., Eissen, J., and Maury, R.C., 1999, The lost Inca Plateau: Cause of flat subduction beneath Peru?: Earth and Planetary Science Letters, v. 171, no. 3, p. 335–341, https://doi.org/10.1016/S0012-821X(99)00153-3.

Gutscher, M., Maury, R.C., Eissen, J., and Bourdon, E., 2000, Can slab melting be caused by flat subduction?: Geology, v. 28, no. 6, p. 535–538, https://doi.org/10.1130/0091-7613(2000)28<535:CSMBCB>2.0.CO;2.

Hao, L.L., Wang, Q., Wyman, D.A., Qi, Y., Ma, L., Huang, F., Zhang, L., Xia, X.P., and Ou, Q., 2018, First identification of mafic igneous enclaves in Miocene lavas of southern Tibet with implications for Indian continental subduction: Geophysical Research Letters, v. 45, p. 8205–8213, https://doi.org/10.1029/2018GL079061.

Hao, L.L., Wang, Q., Wyman, D.A., Yang, J., Huang, F., and Ma, L., 2019a, Crust-mantle mixing and crustal reworking of southern Tibet during Indian continental subduction: Evidence from Miocene high-silica potassic rocks in Central Lhasa block: Lithos, v. 342–343, p. 407–419, https://doi.org/10.1016/j.lithos.2019.05.035.

Hao, L.L., Wang, Q., Wyman, D.A., Ma, L., Wang, J., Xia, X.P., and Ou, Q., 2019b, First identification of postcollisional A-type magmatism in the Himalayan-Tibetan orogen: Geology, v. 47, p. 187–190, https://doi.org/10.1130/G45526.1.

Harris, N., Xu, R., Lewis, C.L., Hawkesworth, C.J., and Zhang, Y., 1988, Isotope geochemistry of the 1985 Tibet Geotraverse, Lhasa to Golmud: Philosophical Transactions of the Royal Society A, v. 327, p. 263–285.

Harrison, T.M., Yin, A., Grove, M., Lovera, O.M., Ryerson, F., and Zhou, X., 2000, The Zedong window: A record of superposed Tetiary convergence in southeastern Tibet: Journal of Geophysical Research, v. 105, p. 19211–19230, https://doi.org/10.1029/2000JB900078.

Hou, Z., Zheng, Y., Zeng, L., Gao, L., Huang, K., Li, W., Li, Q., Fu, Q., Liang, W., and Sun, Q., 2012, Eocene-Oligocene granitoids in southern Tibet: Constraints on crustal anatexis and tectonic evolution of the Himalayan orogeny: Earth and Planetary Science Letters, v. 349–350, p. 38–52, https://doi.org/10.1016/j.epsl.2012.06.030.

685 Hou, Z., Duan, L., Lu, Y., Zheng, Y., Zhu, D., Yang, Z., Yang, Z., Wang, B., Pei, Y., Zhao, Z.,
686 and Mccuaig, T.C., 2015, Lithospheric architecture of the Lhasa Terrane and its control on
687 ore deposits in the Himalayan-Tibetan orogen: Economic Geology and the Bulletin of the
688 Society of Economic Geologists, v. 110, no. 6, p. 1541–1575,
689 https://doi.org/10.2113/econgeo.110.6.1541.
690 Hou, Z.Q., Gao, Y.F., Qu, X.M., Rui, Z.Y., and Mo, X.X., 2004, Origin of adakitic intrusives
691 generated during mid-Miocene east-west extension in southern Tibet: Earth and Planetary
692 Science Letters, v. 220, p. 139–155, https://doi.org/10.1016/S0012-821X(04)00007-X.
693 Houseman, G.A., and Molnar, P., 1997, Gravitational (Rayleigh-Taylor) instability of a layer
694 with non-linear viscosity and convective thinning of continental lithosphere: Geophysical
695 Journal International, v. 128, p. 125–150, https://doi.org/10.1111/j.1365-
696 246X.1997.tb04075.x.
697 Houseman, G.A., McKenzie, D.P., and Molnar, P., 1981, Convective instability of a thickened
698 boundary layer and its relevance for the thermal evolution of continental convergent belts:
699 Journal of Geophysical Research: Solid Earth, v. 86, p. 6115–6132,
700 https://doi.org/10.1029/JB086iB07p06115.
701 Husson, L., Bernet, M., Guillot, S., Huyghe, P., Mugnier, J.-L., Replumaz, A., Robert, X., and
702 Van der Beek, P., 2014, Dynamic ups and downs of the Himalaya: Geology, v. 42, p. 839–
703 842, https://doi.org/10.1130/G36049.1.
704 Ji, W.-Q., Wu, F.-Y., Liu, C.-Z., and Chung, S.-L., 2012, Early Eocene crustal thickening in
705 southern Tibet: New age and geochemical constraints from the Gangdese batholith: Journal
706 of Asian Earth Sciences, v. 53, p. 82–95, https://doi.org/10.1016/j.jseaes.2011.08.020.
707 Ji, W.Q., Wu, F.Y., Chung, S.L., Wang, X.C., Liu, C.Z., Li, Q.L., Liu, Z.-C., Liu, X.-C., and
708 Wang, J.-G., 2016, Eocene Neo-Tethyan slab breakoff constrained by 45 Ma oceanic island
709 basalt-type magmatism in southern Tibet: Geology, v. 44, no. 4, p. 283–286,
710 https://doi.org/10.1130/G37612.1.
711 Jiang, Z.Q., Wang, Q., Wyman, D.A., Li, Z., Yang, J., Shi, X., Ma, L., Tang, G., Gou, G., Jia,
712 X., and Guo, H., 2014, Transition from oceanic to continental lithosphere subduction in
713 southern Tibet: Evidence from the Late Cretaceous-Early Oligocene (~91–30 Ma) intrusive
714 rocks in the Chanang-Zedong area, southern Gangdese: Lithos, v. 196–197, no. 7, p. 213–
715 231, https://doi.org/10.1016/j.lithos.2014.03.001.
716 Kohn, M.J., and Parkinson, C.D., 2002, Petrologic case for Eocene slab breakoff during the
717 Indo-Asian collision: Geology, v. 30, p. 591–594, https://doi.org/10.1130/0091-
718 7613(2002)030<0591:PCFESB>2.0.CO;2.
719 Leary, R., Orme, D.A., Laskowski, A.K., DeCelles, P.G., Kapp, P., Carrapa, B., and Dettinger,
720 M., 2016, Along-strike diachroneity in deposition of the Kailas Formation in central
721 southern Tibet: Implications for Indian slab dynamics: Geosphere, v. 12, p. 1198–1223,
722 https://doi.org/10.1130/GES01325.1.
723 Leary, R.J., Quade, J., DeCelles, P.G., and Reynolds, A., 2017, Evidence from paleosols for low
724 to moderate elevation of the India-Asia suture zone during mid-Cenozoic time: Geology,
725 v. 45, no. 5, p. 399–402, https://doi.org/10.1130/G38830.1.
726 Lee, H.Y., Chung, S.L., Wang, Y.B., Zhu, D.C., Yang, J.H., Song, B., Liu, D.Y., and Wu, F.Y.,
727 2007, Age, petrogenesis and geological significance of the Linzizong volcanic successions
728 in the Linzhou basin, southern Tibet: Evidence from zircon U-Pb dates and Hf isotopes [in
729 Chinese with English abstract]: Yanshi Xuebao, v. 23, p. 493–500.

730 Lee, H.Y., Chung, S.L., Ji, J., Qian, Q., Gallet, S., Lo, C.H., Lee, T.-Y., and Zhang, Q., 2012,
731 Geochemical and Sr-Nd isotopic constraints on the genesis of the Cenozoic Linzizong
732 volcanic successions, southern Tibet: Journal of Asian Earth Sciences, v. 53, no. 2, p. 96–
733 114, https://doi.org/10.1016/j.jseaes.2011.08.019.
734 Lim, C., and Kidd, W.S.F., 2007, Along-strike propagation of slab breakoff at the end of the
735 Taconic orogeny: A model of shortening-extension transition accompanying strike-slip
736 faulting: Geological Society of America Abstracts with Programs, v. 39, no. 7, p. 230.
737 **[[Not cted?]]**Liu, A.L., Wang, Q., Zhu, D.C., Zhao, Z.D., Liu, S.A., Wang, R., Dai, J., Zheng,
738 Y., and Zhang, L., 2018, Origin of the ca. 50 Ma Linzizong shoshonitic volcanic rocks in the
739 eastern Gangdese arc, southern Tibet: Lithos, v. 304–307, p. 374–387,
740 https://doi.org/10.1016/j.lithos.2018.02.017.
741 Liu, D., Zhao, Z., Depaolo, D.J., Zhu, D., Meng, F., Shi, Q., and Wang, Q., 2017, Potassic
742 volcanic rocks and adakitic intrusions in southern Tibet: Insights into mantle-crust
743 interaction and mass transfer from Indian plate: Lithos, v. 268–271, p. 48–64,
744 https://doi.org/10.1016/j.lithos.2016.10.034.
745 Liu, X.H., Xu, Q., and Ding, L., 2016, Differential surface uplift: Cenozoic paleoelevation
746 history of the Tibetan plateau: Science China Earth Sciences, v. 59, no. 11, p. 2105–2120,
747 https://doi.org/10.1007/s11430-015-5486-y.
748 Ma, L., Wang, Q., Li, Z.X., Wyman, D.A., Yang, J.H., Jiang, Z.Q., Liu, Y.S., Gou, G.L., and
749 Guo, H.F., 2017, Subduction of Indian continent beneath southern Tibet in the latest Eocene
750 (~35 Ma): Insights from the Quguosha gabbros in southern Lhasa block: Gondwana
751 Research, v. 41, p. 77–92, https://doi.org/10.1016/j.gr.2016.02.005.
752 Macpherson, C.G., Dreher, S.T., and Thirlwall, M.F., 2006, Adakites without slab melting: High
753 pressure differentiation of island arc magma, Mindanao, the Philippines: Earth and Planetary
754 Science Letters, v. 243, p. 581–593, https://doi.org/10.1016/j.epsl.2005.12.034.
755 Mahéo, G., Guillot, S., Blichert-Toft, J., Rolland, Y., and Pecher, A., 2002, A slab breakoff
756 model for the Neogene thermal evolution of South Karakorum and South Tibet: Earth and
757 Planetary Science Letters, v. 195, p. 45–58, https://doi.org/10.1016/S0012-821X(01)00578-
758 7.
759 Mahéo, G., Blichert-Toft, J., Pin, C., Guillot, S., and Pecher, A., 2009, Partial melting of mantle
760 and crustal sources beneath south Karakorum, Pakistan: Implications for the Miocene
761 geodynamic evolution of the India-Asia Convergence Zone: Journal of Petrology, v. 50,
762 no. 3, p. 427–449, https://doi.org/10.1093/petrology/egp006.
763 Miller, C., Schuster, R., Klötzli, U., Frank, W., and Purtscheller, F., 1999, Post-collisional
764 potassic and ultrapotassic magmatism in SW Tibet: Geochemical and Sr-Nd-Pb-O isotopic
765 constraints for mantle source characteristics and petrogenesis: Journal of Petrology, v. 40,
766 no. 9, p. 1399–1424, https://doi.org/10.1093/petroj/40.9.1399.
767 Mo, X., Hou, Z., Niu, Y., Dong, G., Qu, X., Zhao, Z., and Yang, Z., 2007, Mantle contributions
768 to crustal thickening during continental collision: Evidence from Cenozoic igneous rocks in
769 southern Tibet: Lithos, v. 96, no. 1, p. 225–242, https://doi.org/10.1016/j.lithos.2006.10.005.
770 Mo, X., Niu, Y., Dong, G., Zhao, Z., Hou, Z., Zhou, S., and Ke, S., 2008, Contribution of
771 syncollisional felsic magmatism to continental crust growth: A case study of the Paleogene
772 Linzizong volcanic succession in southern Tibet: Chemical Geology, v. 250, no. 1, p. 49–67,
773 https://doi.org/10.1016/j.chemgeo.2008.02.003.

774 Molnar, P., 1988, A review of geophysical constraints on the deep structure of the Tibetan
775 plateau, the Himalaya and the Karakoram, and their tectonic implications: Philosophical
776 Transactions of the Royal Society A, v. 326, p. 33–88.
777 Molnar, P., England, P., and Martinod, J., 1993, Mantle dynamics, the uplift of the Tibetan
778 plateau, and the Indian monsoon: Reviews of Geophysics, v. 31, p. 357–396,
779 https://doi.org/10.1029/93RG02030.
780 Pan, F.B., Zhang, H.F., Harris, N., Xu, W.C., and Guo, L., 2012, Oligocene magmatism in the
781 eastern margin of the east Himalayan syntaxis and its implication for the India-Asia
782 postcollisional process: Lithos, v. 154, p. 181–192,
783 https://doi.org/10.1016/j.lithos.2012.07.004.
784 Pang, K., Chung, S., Zarrinkoub, M.H., Li, X., Lee, H., Lin, T., and Chiu, H., 2016, New age and
785 geochemical constraints on the origin of Quaternary adakite-like lavas in the Arabia-Eurasia
786 collision zone: Lithos, v. 264, p. 348–359, https://doi.org/10.1016/j.lithos.2016.08.042.
787 Qu, X., Hou, Z., and Li, Y., 2004, Melt components derived from a subducted slab in late
788 orogenic ore-bearing porphyries in the Gangdese copper belt, southern Tibetan plateau:
789 Lithos, v. 74, p. 131–148, https://doi.org/10.1016/j.lithos.2004.01.003.
790 Replumaz, A., Negredo, A.M., Villaseñor, A., and Guillot, S., 2010, Indian continental
791 subduction and slab break-off during Tertiary collision: Terra Nova, v. 22, p. 290–296,
792 https://doi.org/10.1111/j.1365-3121.2010.00945.x.
793 Spicer, R.A., Harris, N.B.W., Widdowson, M., Herman, A., Guo, S., Valdes, P.J., Wolfe, J.A.,
794 and Kelley, S.P., 2003, Constant elevation of southern Tibet over the past 15 million years:
795 Nature, v. 421, p. 622–624, https://doi.org/10.1038/nature01356.
796 Streck, M.J., Leeman, W.P., and Chesley, J.T., 2007, High-magnesian andesite from Mount
797 Shasta: A product of magma mixing and contamination, not a primitive mantle melt:
798 Geology, v. 35, no. 4, p. 351–354, https://doi.org/10.1130/G23286A.1.
799 Su, T., Farnsworth, A., Spicer, R.A., Huang, J., Wu, F., Liu, J., Li, S., Xing, Y., Huang, Y.,
800 Deng, W., Tang, H., Xu, C., Zhao, F., Srivastava, G., Valdes, P.J., Deng, T., and Zhou, Z.,
801 2019, No high Tibetan plateau until the Neogene: Science Advances, v. 5, no. eaav2189,
802 https://doi.org/10.1126/sciadv.aav2189.
803 Sun, S.S., and McDonough, W., 1989, Chemical and isotopic systematics of oceanic basalts:
804 Implications for mantle composition and processes, *in* Saunders, A.D., and Norry, M.J., eds.,
805 1989, Magmatism in the Ocean Basins: Geological Society, London, Special Publication 42,
806 p. 313–345, https://doi.org/10.1144/GSL.SP.1989.042.01.19.
807 Sun, X., Lu, Y.J., McCuaig, T.C., Zheng, Y.Y., Chang, H.F., Guo, F., and Xu, L.J., 2018,
808 Miocene ultrapotassic, high-Mg dioritic, and adakite-like rocks from Zhunuo in Southern
809 Tibet: Implications for mantle metasomatism and porphyry copper mineralization in
810 collisional Orogens: Journal of Petrology, v. 59, no. 3, p. 341–386,
811 https://doi.org/10.1093/petrology/egy028.
812 Turner, S., Sandiford, M., and Foden, J., 1992, Some geodynamic and compositional constraints
813 on postorogenic magmatism: Geology, v. 20, p. 931–934, https://doi.org/10.1130/0091-
814 7613(1992)020<0931:SGACCO>2.3.CO;2.
815 Turner, S., Hawkesworth, C., Liu, J., Rogers, N., Kelley, S., and Calsteren, P., 1993, Timing of
816 Tibetan uplift constrained by analysis of volcanic rocks: Nature, v. 364, p. 50–54,
817 https://doi.org/10.1038/364050a0.
818 Turner, S., Arnaud, N., Liu, J., Rogers, N., Hawkesworth, C., Harris, N., Keller, S., and
819 Calsteren, P., 1996, Post-collision, shoshonitic volcanism on the Tibetan plateau:

Implications for convective thinning of the lithosphere and the source of ocean island basalts: Journal of Petrology, v. 37, no. 1, p. 45–71, https://doi.org/10.1093/petrology/37.1.45.

van der Meulen, M.J., Kouwenhoven, T.J., van der Zwaan, G.J., Meulenkamp, J.E., and Wortel, M.J.R., 1999, Late Miocene uplift in the Romagnan Apennines and the detachment of subducted lithosphere: Tectonophysics, v. 315, p. 319–335, https://doi.org/10.1016/S0040-1951(99)00282-6.

Van der Voo, R., Spakman, W., and Bijwaard, H., 1999, Tethyan subducted slabs under India: Earth and Planetary Science Letters, v. 171, p. 7–20, https://doi.org/10.1016/S0012-821X(99)00131-4.

van Hinsbergen, D.J., Kapp, P., Dupontnivet, G., Lippert, P.C., Decelles, P.G., and Torsvik, T.H., 2011, Restoration of Cenozoic deformation in Asia and the size of Greater India: Tectonics, v. 30, no. 5, https://doi.org/10.1029/2011TC002908.

Wang, Q., Xu, J.F., Jian, P., Bao, Z.W., Zhao, Z.H., Li, C.F., Xiong, X.L., and Ma, J.L., 2006, Petrogenesis of adakitic porphyries in an extensional tectonic setting, Dexing, South China: Implications for the genesis of porphyry copper mineralization: Journal of Petrology, v. 47, p. 119–144, https://doi.org/10.1093/petrology/egi070.

Wang, Q., Wyman, D.A., Xu, J., Dong, Y., Vasconcelos, P.M., Pearson, N.J., Wan, Y., Dong, H., Li, C., Yu, Y., Zhu, T., Feng, X., Zhang, Q., Zi, F., and Chu, Z., 2008, Eocene melting of subducting continental crust and early uplifting of central Tibet: Evidence from central-western Qiangtang high-K calc-alkaline andesites, dacites and rhyolites: Earth and Planetary Science Letters, v. 272, no. 1, p. 158–171, https://doi.org/10.1016/j.epsl.2008.04.034.

Wang, Q., Hawkesworth, C.J., Wyman, D., Chung, S.L., Wu, F.-Y., Li, X., Li, Z., Gou, G., Zhang, X., Tang, G., Dan, W., Ma, L., and Dong, Y., 2016, Pliocene-quaternary crustal melting in central and northern Tibet and insights into crustal flow: Nature Communications, v. 7, no. 11888, https://doi.org/10.1038/ncomms11888.

Wang, R., Weinberg, R., Collins, W., Richards, J., and Zhu, D., 2018, Origin of postcollisional magmas and formation of porphyry Cu deposits in southern Tibet: Earth-Science Reviews, v. 181, p. 122–143, https://doi.org/10.1016/j.earscirev.2018.02.019.

Watts, A.B., 2001, Isostasy and Flexure of the Lithosphere: Cambridge, UK, Cambridge University Press, 508 p.

Webb, A.A.G., Guo, H.C., Clift, P.D., Husson, L., Muller, T., Costantino, D., Yin, A., Xu, Z., Cao, H., and Wang, Q., 2017, The Himalaya in 3D: Slab dynamics controlled mountain building and monsoon intensification: Lithosphere, v. 9, no. 4, p. 637–651, https://doi.org/10.1130/L636.1.

Wen, D.R., Chung, S.L., Song, B., Iizuka, Y., Yang, H.J., Ji, J.Q., Liu, D.Y., and Gallet, S., 2008, Late Cretaceous Gangdese intrusions of adakitic geochemical characteristics, SE Tibet: Petrogenesis and tectonic implications: Lithos, v. 105, p. 1–11, https://doi.org/10.1016/j.lithos.2008.02.005.

Williams, H., Turner, S., Kelley, S., and Harris, N., 2001, Age and composition of dikes in southern Tibet: New constraints on the timing of east-west extension and its relationship to postcollisional volcanism: Geology, v. 29, no. 4, p. 339–342, https://doi.org/10.1130/0091-7613(2001)029<0339:AACODI>2.0.CO;2.

Williams, H.M., Turner, S.P., Pearce, J.A., Kelley, S.P., and Harris, N.B.W., 2004, Nature of the source regions for post-collisional, potassic magmatism in southern and northern Tibet from

geochemical variations and inverse trace element modelling: Journal of Petrology, v. 45, p. 555–607, https://doi.org/10.1093/petrology/egg094.

Xiong, X.L., 2006, Trace element evidence for the growth of early continental crust by melting of rutile-bearing hydrous eclogite: Geology, v. 34, p. 945–948, https://doi.org/10.1130/G22711A.1.

Xu, B., Griffin, W.L., Xiong, Q., Hou, Z., Reilly, S.Y., Guo, Z., Pearson, N., Greau, Y., Yang, Z., and Zheng, Y., 2017, Ultrapotassic rocks and xenoliths from South Tibet: Contrasting styles of interaction between lithospheric mantle and asthenosphere during continental collision: Geology, v. 45, no. 1, p. 51–54, https://doi.org/10.1130/G38466.1.

Xu, W.C., Zhang, H.-F., Guo, L., and Yuan, H.L., 2010, Miocene high Sr/Y magmatism, south Tibet: Product of partial melting of subducted Indian continental crust and its tectonic implication: Lithos, v. 114, p. 293–306, https://doi.org/10.1016/j.lithos.2009.09.005.

[[Not cited? See query in text.]]Yang, Z., Lu, Y., Hou, Z., and Chang, Z., 2015, High-Mg diorite from Qulong in southern Tibet: Implications for the genesis of adakite-like intrusions and associated porphyry Cu deposits in collisional orogens: Journal of Petrology, v. 56, no. 2, p. 227–254, https://doi.org/10.1093/petrology/egu076.

Yin, A., and Harrison, T.M., 2000, Geologic evolution of the Himalayan-Tibetan orogen: Annual Review of Earth and Planetary Sciences, v. 28, p. 211–280, https://doi.org/10.1146/annurev.earth.28.1.211.

Yin, A., Harrison, T., Ryerson, F., Chen, W., Kidd, W., and Copeland, P., 1994, Tertiary structural evolution of the Gangdese thrust system, southeastern Tibet: Journal of Geophysical Research: Solid Earth, v. 99, no. B9, p. 18175–18201, https://doi.org/10.1029/94JB00504.

Yin, A., Harrison, T.M., Murphy, M.A., Grove, M., and Nie, S., 1999, Tertiary deformation history of southeastern and southwestern Tibet during the Indo-Asian collision: Geological Society of America Bulletin, v. 111, no. 11, p. 1644–1664, https://doi.org/10.1130/0016-7606(1999)111<1644:TDHOSA>2.3.CO;2.

Zeng, L.S., Gao, L.E., Xie, K.J., and Zeng, L.J., 2011, Mid-Eocene high Sr/Y granites in the Northern Himalayan gneiss dome: Melting thickened lower continental crust: Earth and Planetary Science Letters, v. 303, p. 251–266, https://doi.org/10.1016/j.epsl.2011.01.005.

[[Not cited?]]Zhang, H.F., Xu, W.C., Guo, J.Q., Zhong, K.Q., Cai, H.M., and Yuan, H.L., 2007, Indosinian orogenesis of the Gangdise Terrane: Evidences from zircon U-Pb dating and petrogenesis of granitoids [in Chinese with English abstract]: Earth Science—Journal of China University of Geosciences, v. 32, p. 155–166.

Zhang, L.Y., Ducea, M.N., Ding, L., Pullen, A., Kapp, P., and Hoffman, D., 2014, Southern Tibetan Oligocene-Miocene adakites: A record of Indian slab tearing: Lithos, v. 210–211, p. 209–223, https://doi.org/10.1016/j.lithos.2014.09.029.

Zhao, Z., Mo, X., Dilek, Y., Niu, Y., DePaolo, D., Robinson, P., Zhu, D., Sun, C., Dong, G., Zhou, S., Luo, Z., and Hou, Z., 2009, Geochemical and Sr-Nd-Pb-O isotopic compositions of the postcollisional ultrapotassic magmatism in SW Tibet: Petrogenesis and implications for India intra-continental subduction beneath southern Tibet: Lithos, v. 113, no. 1–2, p. 190–212, https://doi.org/10.1016/j.lithos.2009.02.004.

Zheng, Y.C., Hou, Z.Q., Li, W., Liang, W., Huang, K.X., Li, Q.Y., Sun, Q.Z., Fu, Q., and Zhang, S., 2012, Petrogenesis and geological implications of the Oligocene Chongmuda-Mingze adakite-like intrusions and their mafic enclaves, southern Tibet: The Journal of Geology, v. 120, p. 647–669, https://doi.org/10.1086/667812.

Zheng, Y.F., 2019, Subduction zone geochemistry: Geoscience Frontiers, v. 10, p. 1223–1254, https://doi.org/10.1016/j.gsf.2019.02.003.

Zhou, S., Mo, X., Zhao, Z., Qiu, R., Niu, Y., Guo, T., and Zhang, S., 2010, $^{40}Ar/^{39}Ar$ geochronology of post-collisional volcanism in the middle Gangdese belt, southern Tibet: Journal of Asian Earth Sciences, v. 37, no. 3, p. 246–258, https://doi.org/10.1016/j.jseaes.2009.08.011.

Zhu, D., Wang, Q., Zhao, Z., Chung, S., Cawood, P.A., Niu, Y., Liu, S., Wu, F., and Mo, X., 2015, Magmatic record of India-Asia collision: Scientific Reports, v. 5, no. 1, p. 14289–14289, https://doi.org/10.1038/srep14289.

Zhu, D.C., Zhao, Z.D., Niu, Y., Dilek, Y., Wang, Q., Ji, W.H., Dong, G.C., Sui, Q.L., Liu, Y.S., and Yuan, H.L., 2012, Cambrian bimodal volcanism in the Lhasa Terrane, southern Tibet: Record of an early Paleozoic Andean-type magmatic arc in the Australian proto-Tethyan margin: Chemical Geology, v. 328, p. 290–308, https://doi.org/10.1016/j.chemgeo.2011.12.024.

Zhu, D.C., Zhao, Z.D., Niu, Y.L., Dilek, Y., Hou, Z.Q., and Mo, X.X., 2013, The origin and pre-Cenozoic evolution of the Tibetan plateau: Gondwana Research, v. 23, p. 1429–1454, https://doi.org/10.1016/j.gr.2012.02.002.

Zhu, D.C., Wang, Q., Cawood, P.A., Zhao, Z.D., and Mo, X.X., 2017, Raising the Gangdese Mountains in southern Tibet: Journal of Geophysical Research: Solid Earth, v. 122, p. 214–223, https://doi.org/10.1002/2016JB013508.

Figure 1. (A) Sketch map shows the location of Tibet in a regional context. (B) Simplified geologic map shows outcrops of magmatic rocks in southern Tibet (Lhasa and Himalaya blocks), modified from Chung et al. (2009), Hou et al. (2015), and Ma et al. (2017). BNS—Bangong-Nujiang suture; SNMZ—ShiquanRiver-NamTso mélange zone; LMF—Luobadui-Milashan Fault; IYZS—Indus-YarlungZangbu suture; STDS—South Tibet Detachment System; MCT—Main Central Thrust; MBT—Main Boundary Thrust. The numbers in the figure are ages of representative post-collisional magmatic rocks (Ma). The Lhasa block can be divided into western and eastern segments (i.e., western Lhasa block, eastern Lhasa block) at 87°E. (C) Simplified geological map of the Wuyu area (modified from Zhou et al., 2010) showing sample locations. The Eocene samples were collected from one location and the Miocene samples were collected from six locations along a stratigraphic section; the detailed GPS coordinates are shown in the Appendix. LVS—Linzizong volcanic successions; GF—Gazhacun Formation; ZF—Zongdangcun Formation; Q—Quaternary sediment.

Figure 2. (A–C) Representative field photographs and (D–F) photomicrographs of the Wuyu Cenozoic lavas. (D) Eocene trachyandesite NML01-1. (E) Miocene rhyolite NML03-1. (F) Miocene dacite NML04-1. Pl—plagioclase; Bi—biotite; Qtz—quartz.

Figure 3. (A–C) Laser altimetry-inductively coupled plasma-mass spectrometry zircon U-Pb Concordia diagrams with representative zircon cathodoluminescence images of the Wuyu Cenozoic lavas are shown. The yellow circles denote the analytical spots of U-Pb dating and Lu-Hf isotopes. The yellow lines represent 100 um. The inserts are the plots of the weighted mean ages. (D) Laser altimetry-multicollector-inductively coupled plasma-mass spectrometry zircon Hf isotopes of the Wuyu Cenozoic lavas. The Linzizong volcanic successions (Lee et al., 2007) and post-collisional adakites (Chung et al., 2009; Xu et al., 2010; Zhang et al., 2014) and ultrapotassic lavas (Liu et al., 2017) were plotted for comparison. CHUR—chondritic uniform reservoir; MSWD—mean square of weighted deviates.

Figure 4. Major element diagrams for the Wuyu lavas are shown. (A–C) SiO_2 versus Na_2O + K_2O, K_2O, and K_2O/Na_2O, respectively. Indian Eocene adakites are from Zeng et al. (2011) and Hou et al. (2012). Pana Formation calc-alkaline rock suite is from Lee et al. (2012). Post-collisional adakitic and ultrapotassic rocks are from Turner et al. (1996), Williams et al. (2001, 2004), Ding et al. (2003), Guo et al. (2015), and Hao et al. (2019b) and references therein.

Figure 5. Major-element Harker diagrams for the Pana Formation calc-alkaline rock suite and Wuyu Eocene lavas are shown.

Figure 6. (A) Chondrite-normalized rare earth element diagram is shown; (B) primitive mantle-normalized trace-element distribution pattern diagram for the Wuyu lavas; (C) Y versus Sr/Y; (D) Yb_N versus $(La/Yb)_N$ where N indicates chondrite normalized. Chondrite and primitive mantle normalization values are from Sun and McDonough (1989). ADR—**[[Define.]] [[Explain what is shown by circles and triangles.]]**

Figure 7. (A–B) SiO_2 versus $^{87}Sr/^{86}Sr(i)$ and $^{143}Nd/^{144}Nd(i)$ diagrams are shown, respectively. (C–D) Plots of $^{87}Sr/^{86}Sr(i)$ versus εNd(t) for Wuyu Cenozoic rocks. All isotopic values were corrected to 12 Ma for comparison. Lhasa crustal basement (Cambrian Amdo orthogneisses and Nima metabasalts) is from Harris et al. (1988) and Zhu et al. (2012). Indian upper crust and Himalaya leucogranites are after Zhang et al. (2014). Indian amphibolites and Eocene adakites are from Zeng et al. (2011) and Hou et al. (2012). Neo-Tethys oceanic subduction-related Lhasa juvenile crust is from Zhang et al. (2014) and Wen et al. (2008). Pre-collisional (80 Ma) adakitic rocks in the Lhasa block are from Wen et al. (2008).

Figure 8. Shown are: (A) SiO_2 versus Eu anomaly; (B) La versus La/Yb; (C) SiO_2 versus Dy/Yb; (D) SiO_2 versus MgO (after Wang et al., 2006). **[[Explain what is shown by circles and triangles.]]**

Figure 9. Cartoon illustrates the tectonic model for eastern Lhasa block post-collisional adakitic magmatism (not to scale). Annotations ①②③ indicate partial melting of Indian continental crust induced by asthenospheric mantle upwelling during Indian continental slab break-off, of Asian mantle wedge metasomatized by subducted Indian crust-released melts and fluids, and of thickened and mixed lower crust (underplated magmas and juvenile crust) caused by the intrusion of mantle melts into the crust, respectively. Magma underplating and tectonic shortening contributed to crustal thickening.

Figure 10. Cartoon diagrams show Indian continental subduction during the post-collisional stage (not to scale). (A) Indian continental slab subduction segmentation after oceanic slab break-off, i.e., low-angle subduction and high-angle subduction beneath western Lhasa block and eastern Lhasa block, respectively (modified from Gutscher et al., 1999). (B) The lateral propagation of Indian slab break-off from both west and east across southern Tibet (modified from Webb et al., 2017, and Leary et al., 2016). Significantly, break-off of Indian continental slab beneath the western Lhasa block may propagate more rapidly than that beneath the eastern Lhasa block (Webb et al., 2017; Hao et al., 2019b). **[[Part A says: during 40~30-25 Ma. Please revise.]]**

Figure 11. La/Yb versus Sr/Y (Wang et al., 2016) diagram shows the effects of residual garnet and plagioclase during partial melting (see text for discussion). F1—adakitic melts derived from eclogitic rocks in the stability field of garnet with little or no plagioclase. F2—crustal melts in the stability field of plagioclase and garnet. F3—crustal melts in the stability field of plagioclase with little or no garnet. **[[Explain what circles and triangles represent.]]**

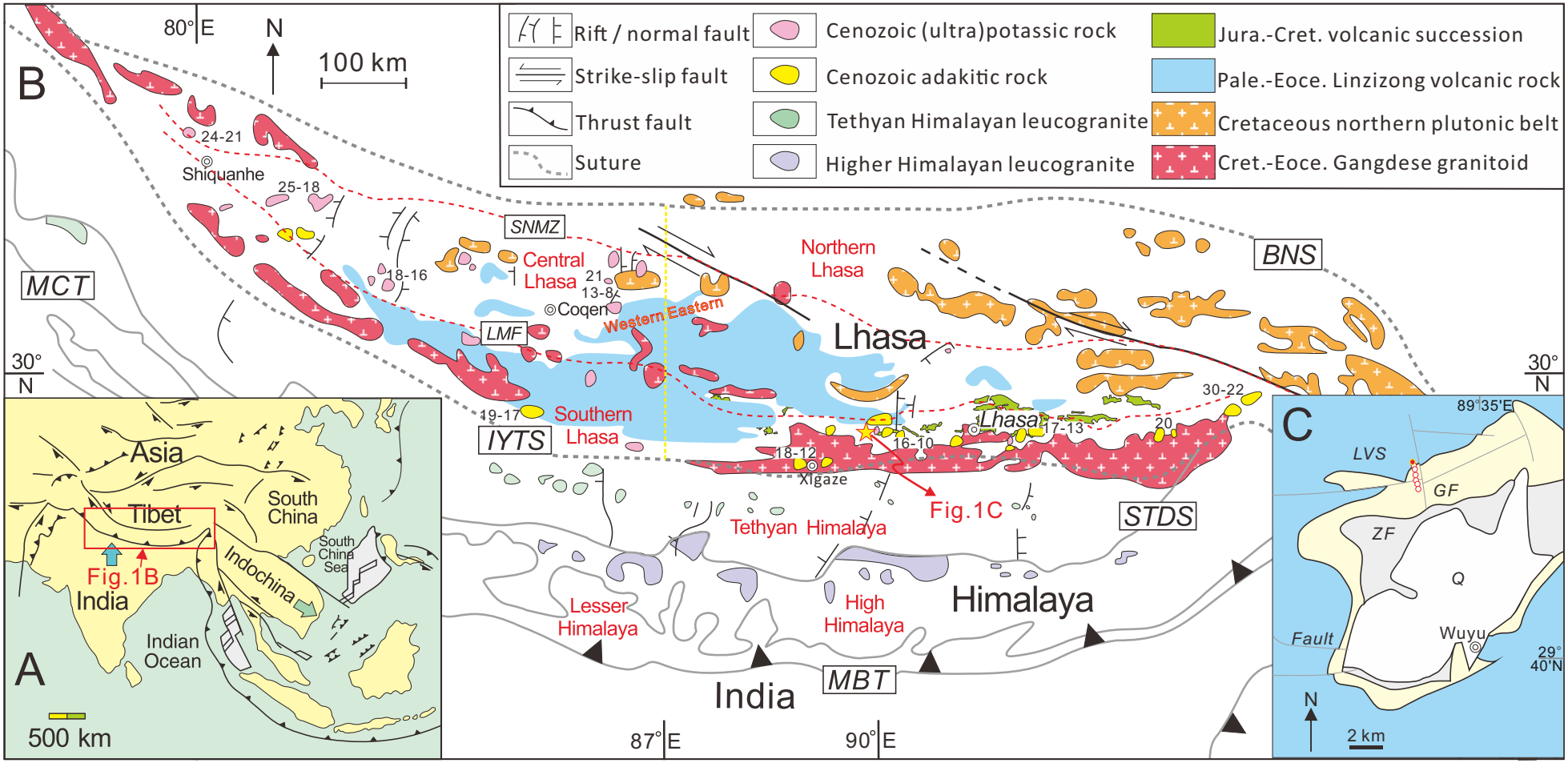
B
80° E
N
100 km
Rift / normal fault
Strike-slip fault
Thrust fault
Suture
Cenozoic (ultra)potassic rock
Cenozoic adakitic rock
Tethyan Himalayan leucogranite
Higher Himalayan leucogranite
Jura.-Cret. volcanic succession
Pale.-Eoce. Linzizong volcanic rock
Cretaceous northern plutonic belt
Cret.-Eoce. Gangdese granitoid
24-21
Shiquanhe
25-18
18-16
SNMZ
Central Lhasa
21
13-8
Coqen
Western
Eastern
LMF
Northern Lhasa
Lhasa
BNS
MCT
30° N
30° N
19-17
Southern Lhasa
IYTS
16-10
18-12
Xigaze
Lhasa
17-13
20
30-22
Fig.1C
STDS
Tethyan Himalaya
Lesser Himalaya
High Himalaya
Himalaya
India
MBT
87° E
90° E
A
Asia
Tibet
South China
Fig.1B
India
Indochina
South China Sea
Indian Ocean
500 km
C
89°35'E
LVS
GF
ZF
Q
Fault
Wuyu
29° 40'N
N
2 km

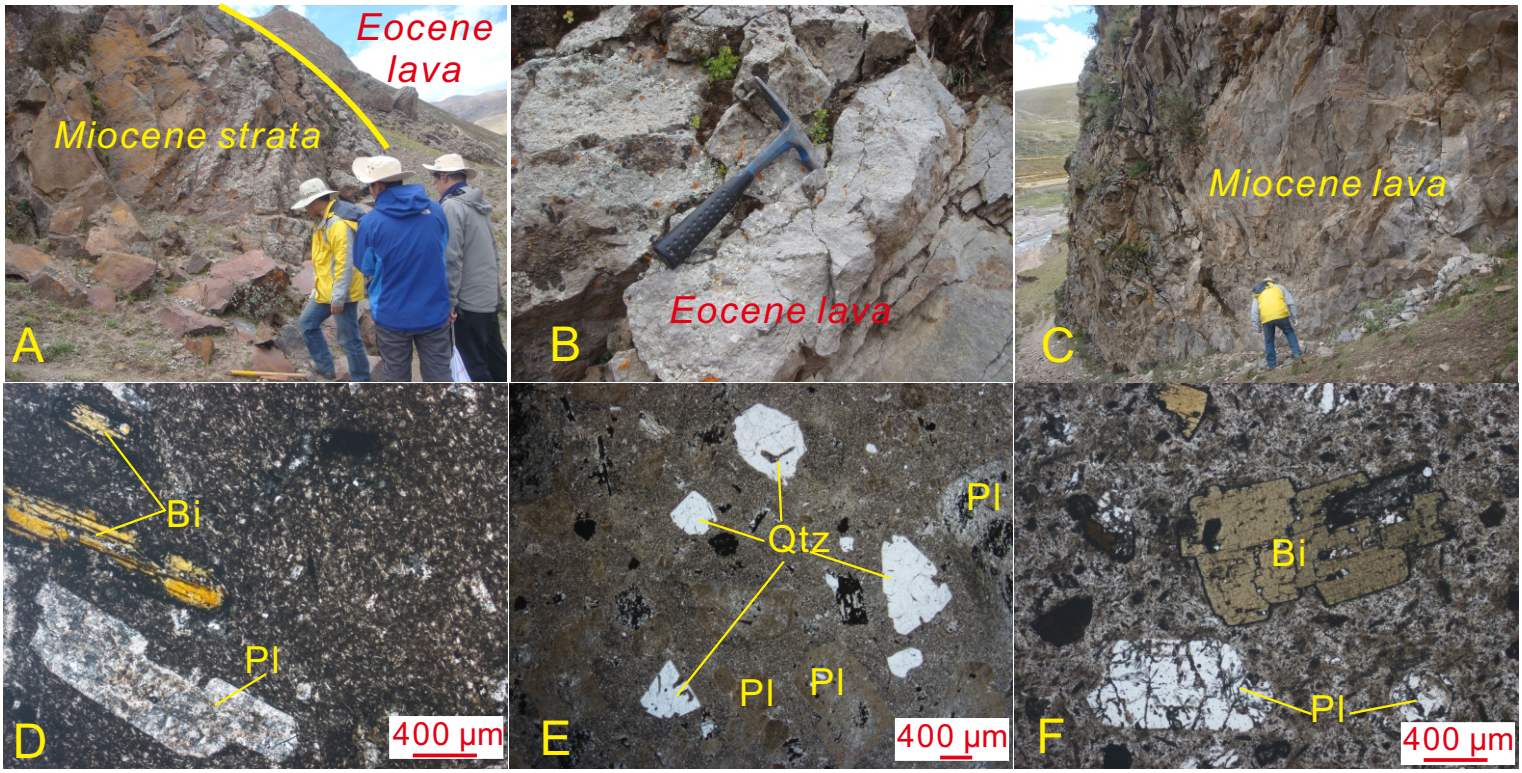
Eocene
lava
Miocene strata
A
Eocene lava
B
Miocene lava
C
Bi
Pl
D
400 μm
Pl
Qtz
Pl
Pl
E
400 μm
Bi
Pl
F
400 μm

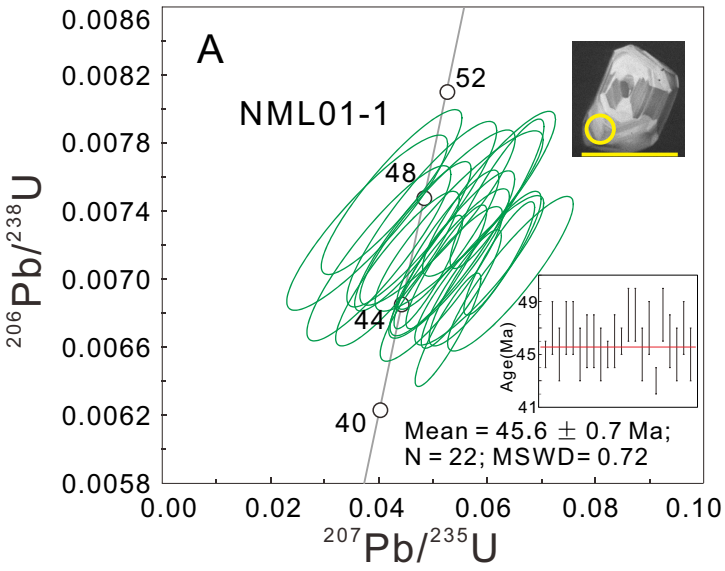
A
NML01-1
52
48
44
40
Mean = 45.6 ± 0.7 Ma;
N = 22; MSWD= 0.72
Age(Ma)
49
45
41
0.0086
0.0082
0.0078
0.0074
0.0070
0.0066
0.0062
0.0058
0.00
0.02
0.04
0.06
0.08
0.10
206Pb/238U
207Pb/235U

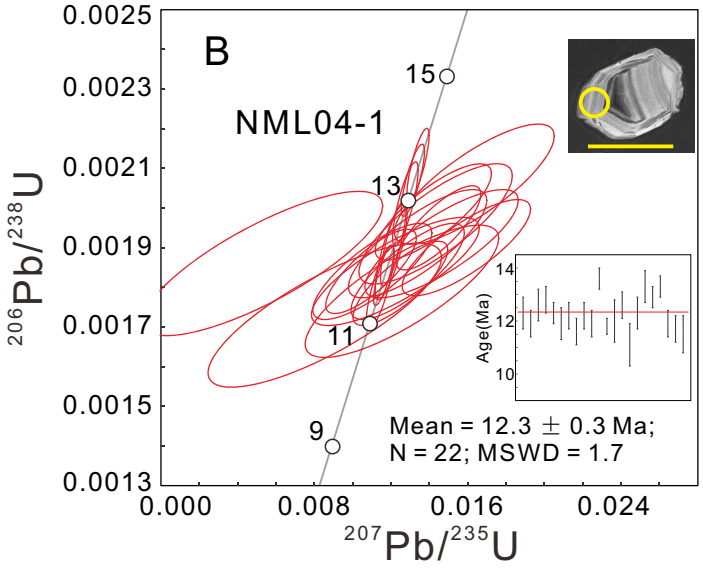
B
NML04-1
15
13
11
9
Mean = 12.3 ± 0.3 Ma;
N = 22; MSWD = 1.7
Age(Ma)
14
12
10
0.0025
0.0023
0.0021
0.0019
0.0017
0.0015
0.0013
0.000
0.008
0.016
0.024
206Pb/238U
207Pb/235U

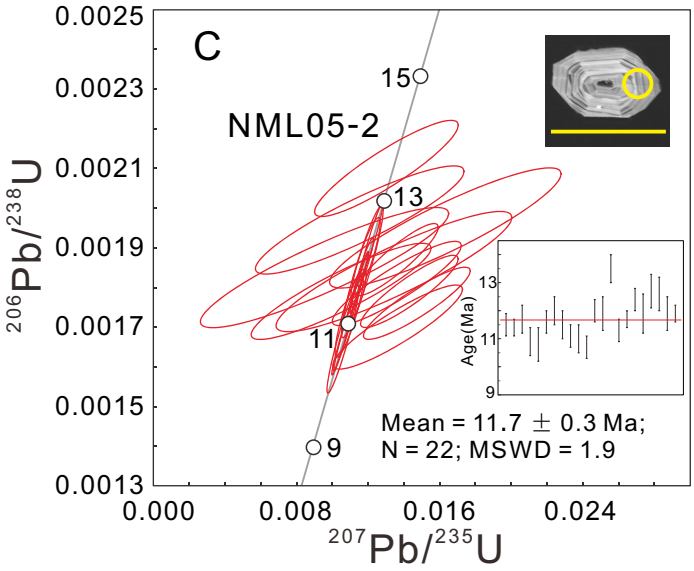
C
NML05-2
15
13
11
9
Mean = 11.7 ± 0.3 Ma;
N = 22; MSWD = 1.9
Age(Ma)
13
11
9
0.0025
0.0023
0.0021
0.0019
0.0017
0.0015
0.0013
0.000
0.008
0.016
0.024
206Pb/238U
207Pb/235U

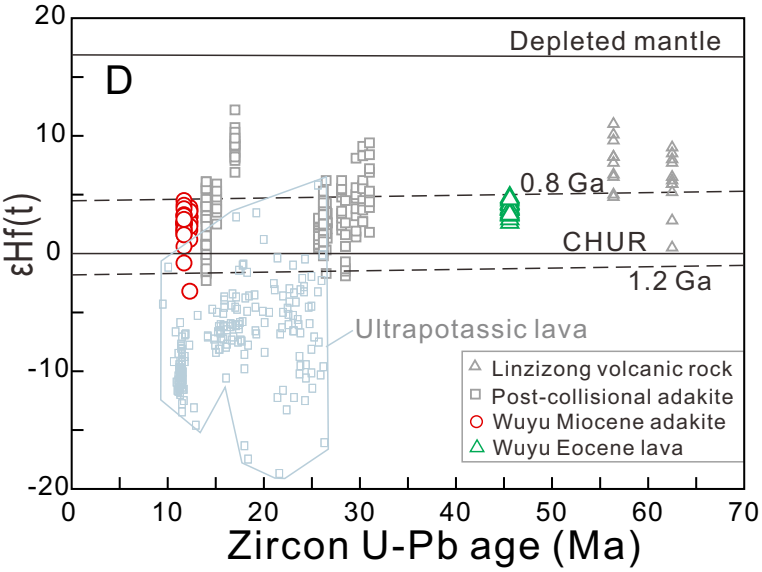
D
Depleted mantle
0.8 Ga
CHUR
1.2 Ga
Ultrapotassic lava
Linzizong volcanic rock
Post-collisional adakite
Wuyu Miocene adakite
Wuyu Eocene lava
20
10
0
-10
-20
εHf(t)
0
10
20
30
40
50
60
70
Zircon U-Pb age (Ma)

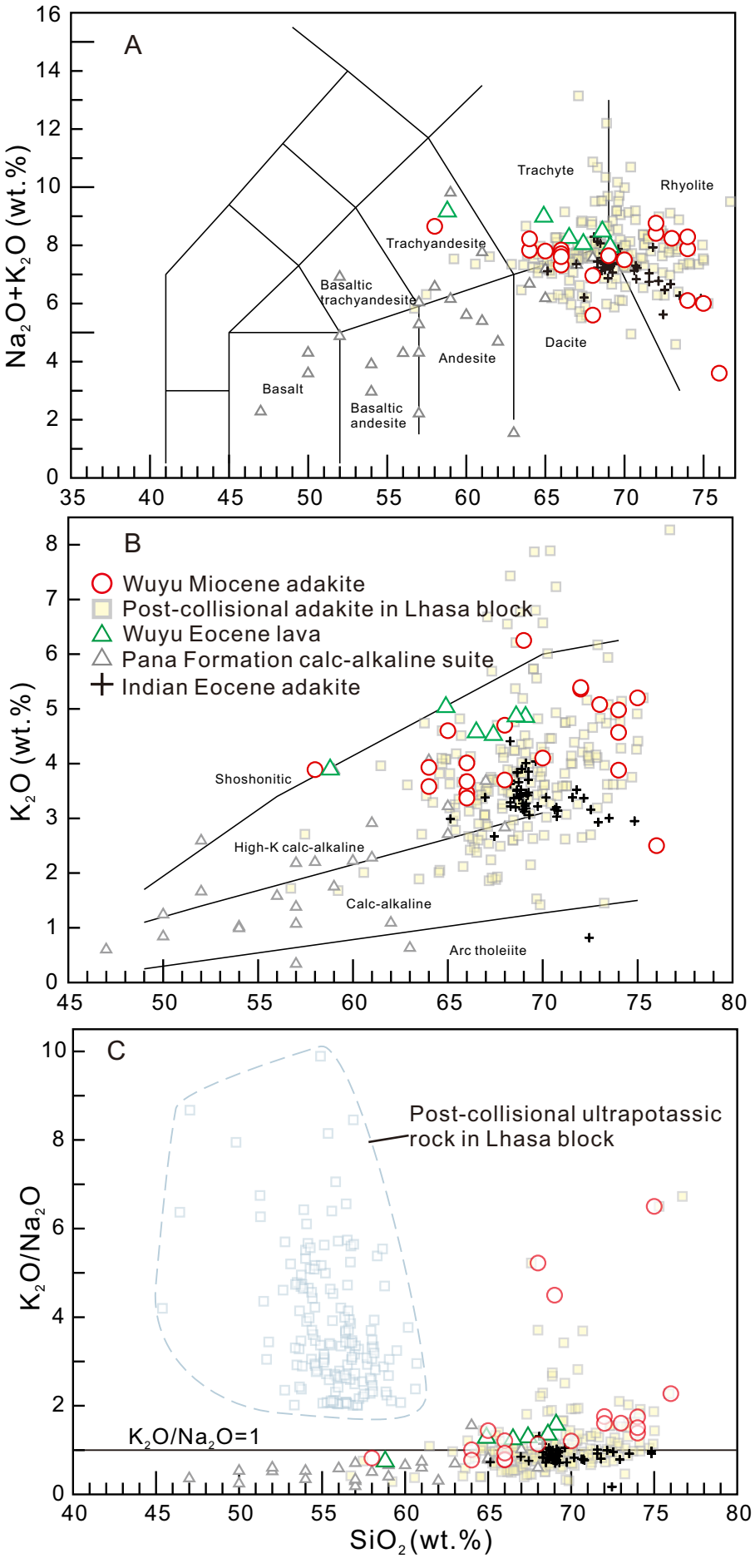
A
Trachyte
Rhyolite
Trachyandesite
Basaltic trachyandesite
Andesite
Dacite
Basalt
Basaltic andesite
Na2O+K2O (wt.%)
B
Wuyu Miocene adakite
Post-collisional adakite in Lhasa block
Wuyu Eocene lava
Pana Formation calc-alkaline suite
Indian Eocene adakite
Shoshonitic
High-K calc-alkaline
Calc-alkaline
Arc tholeiite
K2O (wt.%)
C
Post-collisional ultrapotassic rock in Lhasa block
K2O/Na2O=1
K2O/Na2O
SiO2 (wt.%)

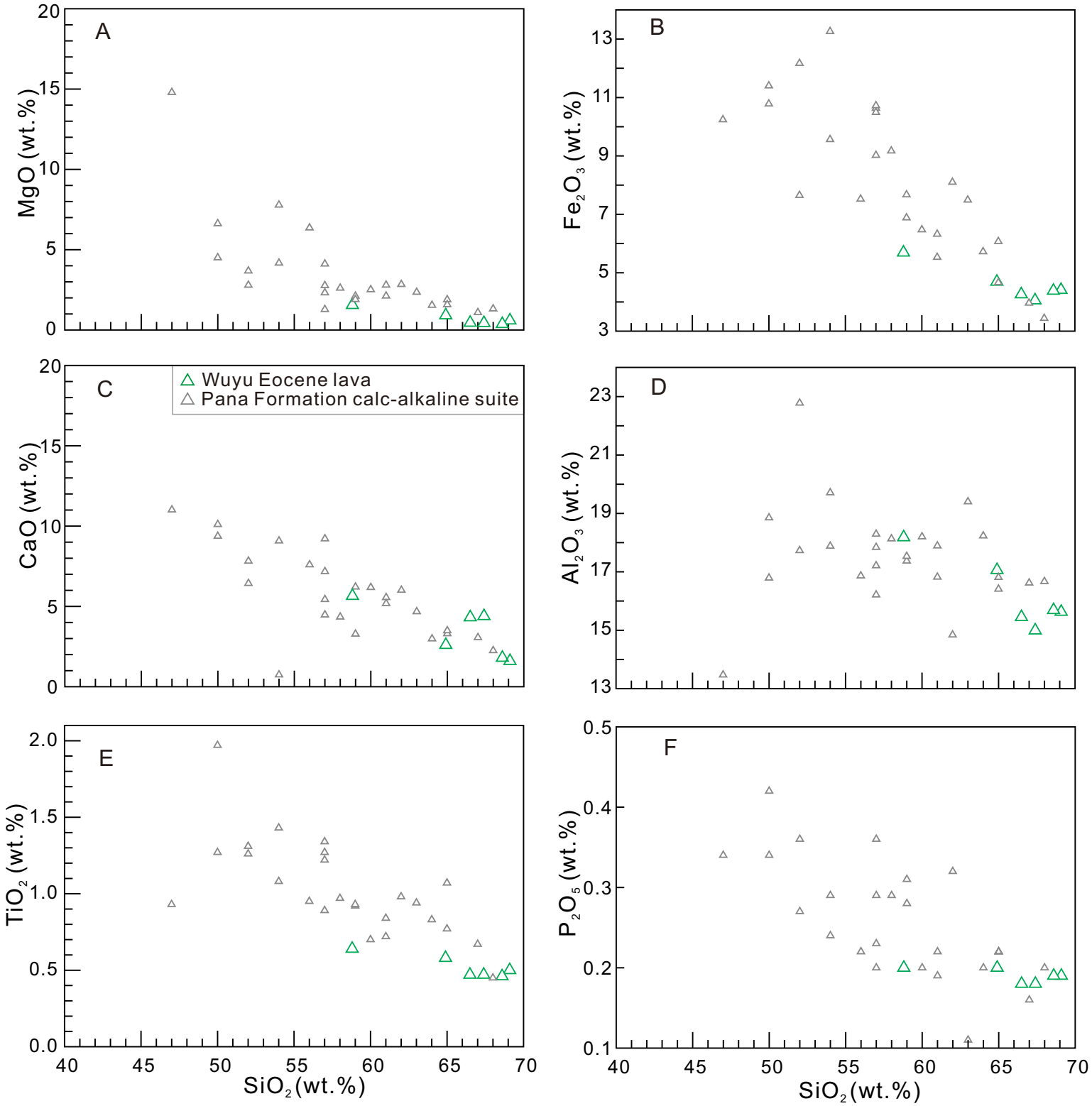
A
MgO (wt.%)
B
Fe_2O_3 (wt.%)
C
CaO (wt.%)
Wuyu Eocene lava
Pana Formation calc-alkaline suite
D
Al_2O_3 (wt.%)
E
TiO_2 (wt.%)
F
P_2O_5 (wt.%)
SiO_2(wt.%)
SiO_2(wt.%)

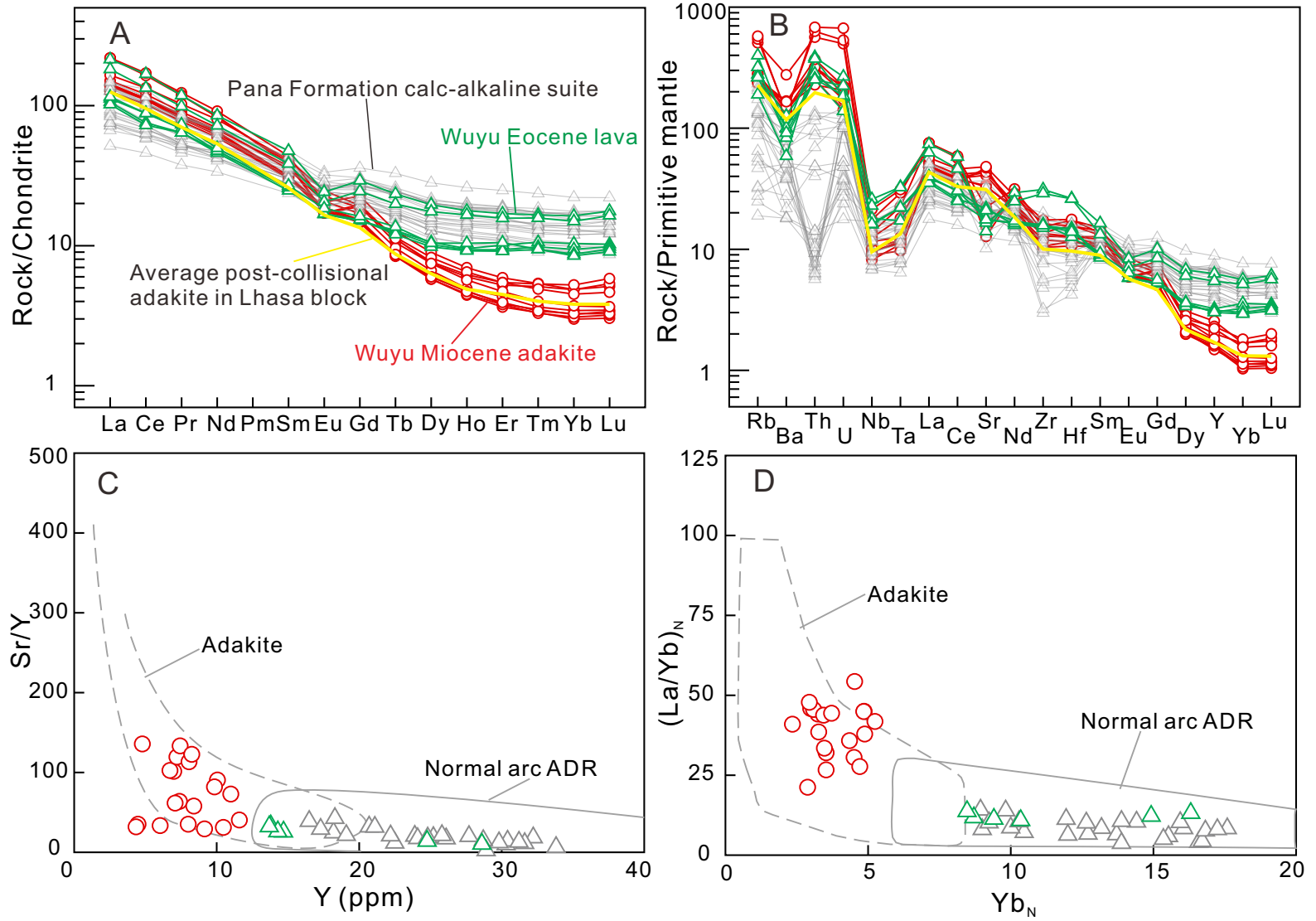
A
Pana Formation calc-alkaline suite
Wuyu Eocene lava
Average post-collisional
adakite in Lhasa block
Wuyu Miocene adakite
Rock/Chondrite
100
10
1
La Ce Pr Nd Pm Sm Eu Gd Tb Dy Ho Er Tm Yb Lu
B
Rock/Primitive mantle
1000
100
10
1
Rb Ba Th U Nb Ta La Ce Sr Nd Zr Hf Sm Eu Gd Dy Y Yb Lu
C
Sr/Y
500
400
300
200
100
0
Adakite
Normal arc ADR
0 10 20 30 40
Y (ppm)
D
(La/Yb)N
125
100
75
50
25
0
Adakite
Normal arc ADR
0 5 10 15 20
YbN

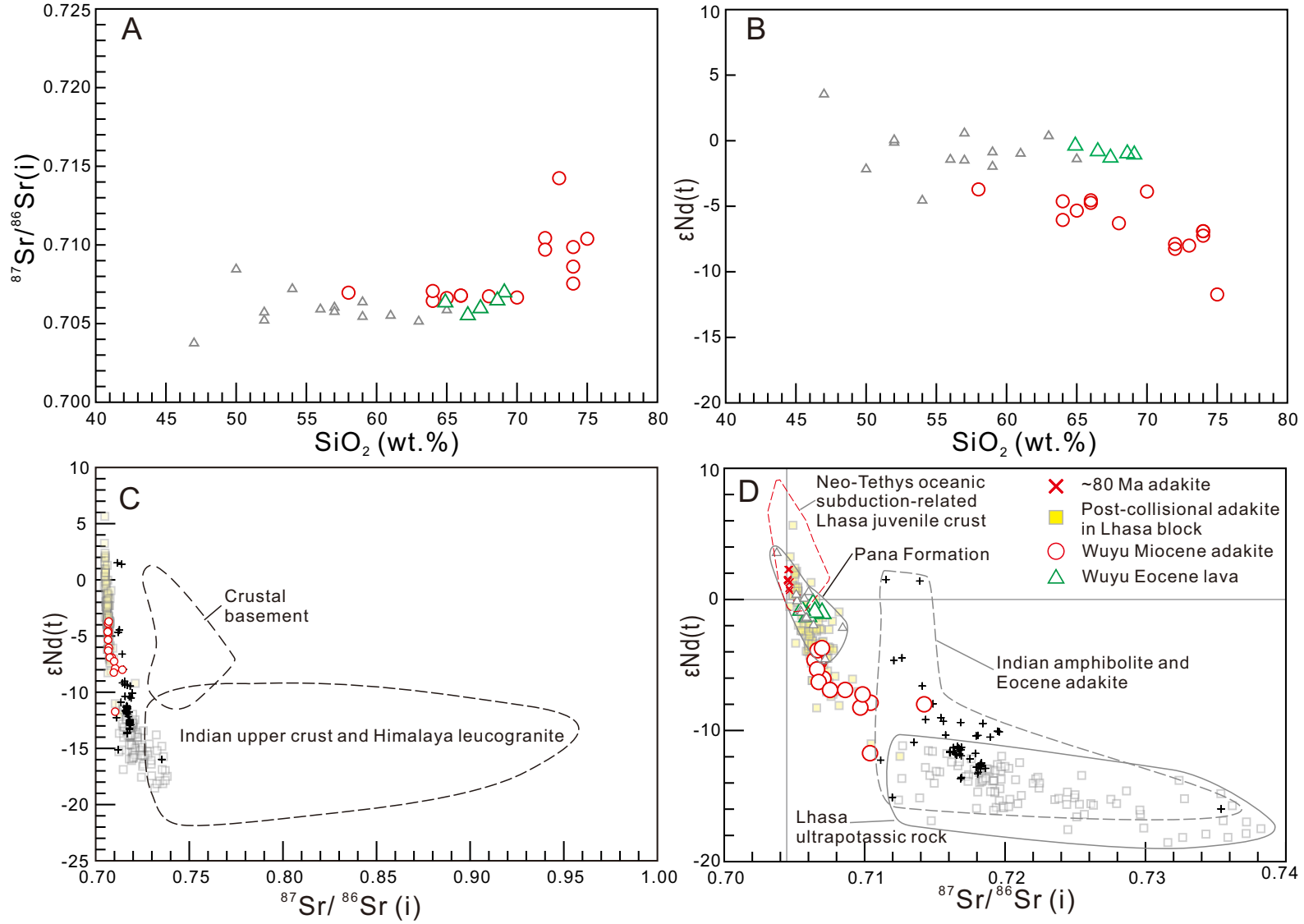
A
$^{87}Sr/^{86}Sr(i)$
SiO_2 (wt.%)
B
εNd(t)
SiO_2 (wt.%)
C
εNd(t)
Crustal basement
Indian upper crust and Himalaya leucogranite
$^{87}Sr/^{86}Sr$ (i)
D
εNd(t)
Neo-Tethys oceanic subduction-related Lhasa juvenile crust
Pana Formation
Indian amphibolite and Eocene adakite
Lhasa ultrapotassic rock
~80 Ma adakite
Post-collisional adakite in Lhasa block
Wuyu Miocene adakite
Wuyu Eocene lava
$^{87}Sr/^{86}Sr$ (i)

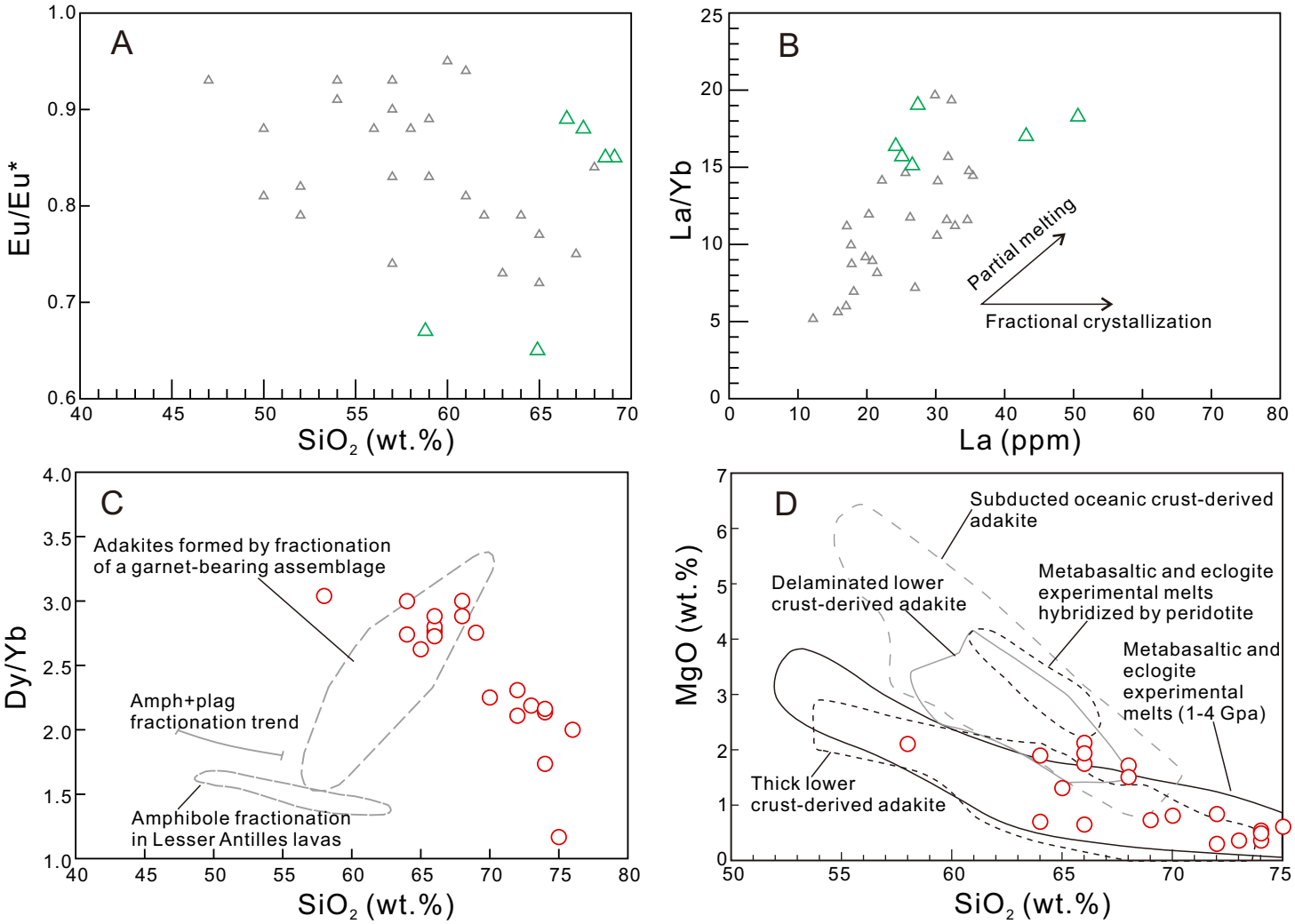
A
Eu/Eu*
SiO2 (wt.%)
B
La/Yb
La (ppm)
Partial melting
Fractional crystallization
C
Dy/Yb
SiO2 (wt.%)
Adakites formed by fractionation
of a garnet-bearing assemblage
Amph+plag
fractionation trend
Amphibole fractionation
in Lesser Antilles lavas
D
MgO (wt.%)
SiO2 (wt.%)
Subducted oceanic crust-derived
adakite
Delaminated lower
crust-derived adakite
Metabasaltic and eclogite
experimental melts
hybridized by peridotite
Metabasaltic and
eclogite
experimental
melts (1-4 Gpa)
Thick lower
crust-derived adakite

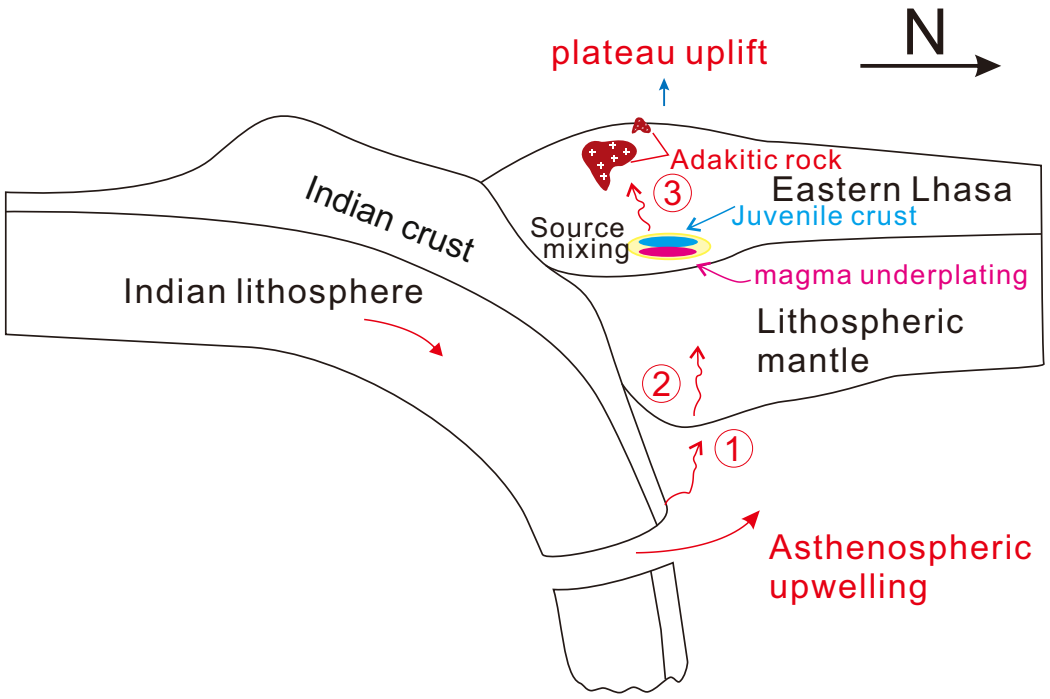
plateau uplift
N
Adakitic rock
Eastern Lhasa
3
Source
mixing
Juvenile crust
magma underplating
Indian crust
Indian lithosphere
Lithospheric
mantle
2
1
Asthenospheric
upwelling

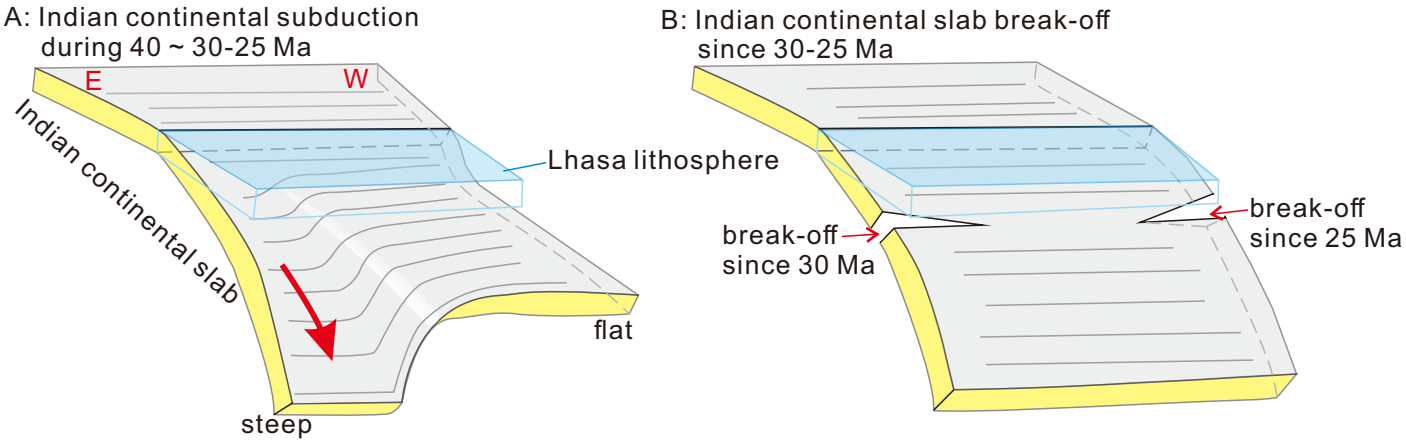
A: Indian continental subduction
during 40 ~ 30-25 Ma
E
W
Indian continental slab
Lhasa lithosphere
flat
steep
B: Indian continental slab break-off
since 30-25 Ma
break-off
since 30 Ma
break-off
since 25 Ma

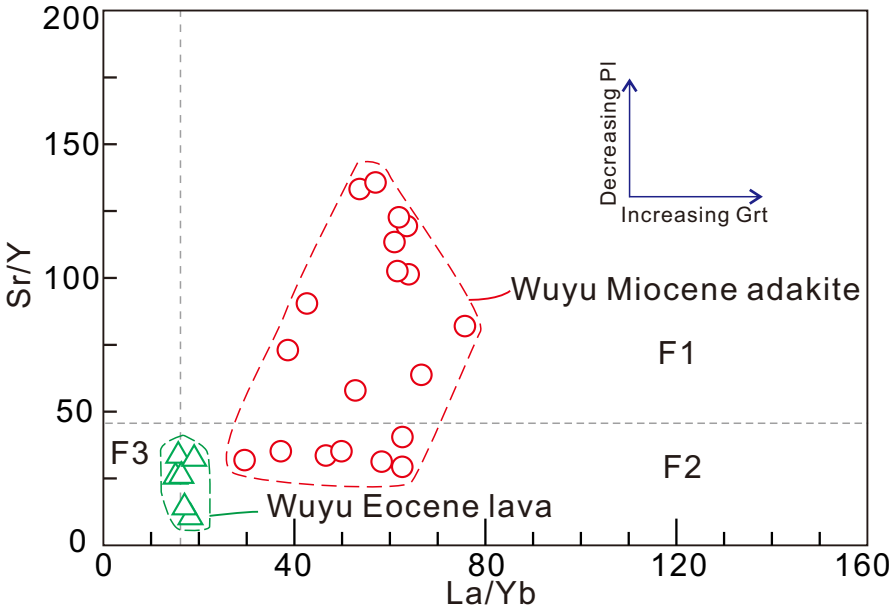
200
150
100
50
0
Sr/Y
0
40
80
120
160
La/Yb
Decreasing PI
Increasing Grt
Wuyu Miocene adakite
F1
F2
F3
Wuyu Eocene lava